Article

TRANSPARENT PROCESS

THE EMBO JOURNAL

# APC/C$^{Cdh1}$ controls CtIP stability during the cell cycle and in response to DNA damage

Lorenzo Lafranchi[1,†], Harmen R de Boer[2,†], Elisabeth GE de Vries[2], Shao-En Ong[3], Alessandro A Sartori[1,*] & Marcel ATM van Vugt[2,**]

## Abstract

**Human cells have evolved elaborate mechanisms for responding to DNA damage to maintain genome stability and prevent carcinogenesis. For instance, the cell cycle can be arrested at different stages to allow time for DNA repair. The APC/C$^{Cdh1}$ ubiquitin ligase mainly regulates mitotic exit but is also implicated in the DNA damage-induced $G_2$ arrest. However, it is currently unknown whether APC/C$^{Cdh1}$ also contributes to DNA repair. Here, we show that Cdh1 depletion causes increased levels of genomic instability and enhanced sensitivity to DNA-damaging agents. Using an integrated proteomics and bioinformatics approach, we identify CtIP, a DNA-end resection factor, as a novel APC/C$^{Cdh1}$ target. CtIP interacts with Cdh1 through a conserved KEN box, mutation of which impedes ubiquitylation and downregulation of CtIP both during $G_1$ and after DNA damage in $G_2$. Finally, we find that abrogating the CtIP–Cdh1 interaction results in delayed CtIP clearance from DNA damage foci, increased DNA-end resection, and reduced homologous recombination efficiency. Combined, our results highlight the impact of APC/C$^{Cdh1}$ on the maintenance of genome integrity and show that this is, at least partially, achieved by controlling CtIP stability in a cell cycle- and DNA damage-dependent manner.**

**Keywords** Cdh1; cell cycle; CtIP; DNA damage; DNA double-strand break repair

**Subject Categories** Cell Cycle; DNA Replication, Repair & Recombination; Post-translational Modifications, Proteolysis & Proteomics

**DOI** 10.15252/embj.201489017 | Received 16 May 2014 | Revised 7 September 2014 | Accepted 30 September 2014 | Published online 27 October 2014

**The EMBO Journal (2014) 33: 2860–2879**

## Introduction

Our genome is constantly exposed to various forms of endogenous and exogenous insults provoking different types of DNA lesions, which can promote tumorigenesis. To maintain genomic integrity, the DNA damage response (DDR) activates cell cycle checkpoints to slow cell cycle progression, thereby allowing time for appropriate repair (Jackson & Bartek, 2009). DNA double-strand breaks (DSBs) are the most cytotoxic lesions induced by ionizing radiation (IR) and certain anticancer drugs. Cells have evolved two major DSB repair mechanisms: non-homologous end-joining (NHEJ) and homologous recombination (HR) (Lieber, 2010).

In the $G_0/G_1$ phase of the cell cycle, NHEJ is the preferred mechanism for DSB repair (Lieber, 2010). In this process, DNA ends are joined without the requirement for a homologous sequence, making NHEJ potentially mutagenic. In contrast, cells that have entered S phase can use the sister chromatid as a template for high-fidelity DSB repair through HR (Aylon *et al*, 2004; Ferreira & Cooper, 2004; Sonoda *et al*, 2006). NHEJ and HR are mutually exclusive pathways since DNA-end resection, which generates long stretches of single-stranded DNA (ssDNA), commits cells to HR and prevents repair by NHEJ. Mechanisms controlling DSB repair pathway choice are under vigorous investigation (Chapman *et al*, 2012). The temporal restriction of HR repair to $S/G_2$ is controlled both at the transcriptional and post-transcriptional level. The expression of many HR factors including Rad51, Rad54, and Brca1 is cell cycle-dependent, being much lower in $G_0/G_1$ than in $S/G_2$ (Gudas *et al*, 1996; Yamamoto *et al*, 1996). In addition, cyclin-dependent kinases (CDKs), core components of the cell cycle machinery, play an important role in DSB repair pathway choice through phosphorylation of multiple HR components, including members of the MRN complex as well as Brca1 and Brca2 (Esashi *et al*, 2005; Ayoub *et al*, 2009; Falck *et al*, 2012). CDK-mediated regulation of DSB repair occurs mainly at the level of DNA-end resection (Aylon *et al*, 2004; Ira *et al*, 2004; Henderson *et al*, 2006; Jazayeri *et al*, 2006; Johnson *et al*, 2011). Human CtIP is essential for the initiation of DNA-end resection, and its function in this process is controlled by various post-translational modifications including phosphorylation, ubiquitylation, and acetylation (Sartori *et al*, 2007; Huertas & Jackson, 2009; Kaidi *et al*, 2010; Steger *et al*, 2013).

Likewise, targeted proteolysis through the ubiquitin-proteasome system (UPS) is a highly regulated process that allows the removal of potentially harmful proteins, thereby restricting their activity. The anaphase-promoting complex/cyclosome (APC/C) is an E3 ubiquitin

1 Institute of Molecular Cancer Research, University of Zurich, Zurich, Switzerland
2 Department of Medical Oncology, University Medical Center Groningen, University of Groningen, Groningen, The Netherlands
3 Department of Pharmacology, University of Washington, Seattle, WA, USA
*Corresponding author. Tel: +41 446353473; Fax: +41 446353484; E-mail: sartori@imcr.uzh.ch
**Corresponding author. Tel: +31 50 3619554; Fax: +31 50 3614862; E-mail: m.vugt@umcg.nl
†These authors contributed equally to this work

ligase involved in cell cycle regulation and becomes activated upon sequential binding to the Cdc20 and Cdh1 adaptor proteins (Peters, 2006; Pesin & Orr-Weaver, 2008). Cdc20 is associated with the APC/C during early mitosis and principally regulates mitotic progression, whereas Cdh1 interacts with the APC/C from late mitosis onwards until the following $G_1$/S transition (Kramer *et al*, 2000; Peters, 2006). In most cases, APC/C$^{Cdh1}$ interacts with its substrates through the recognition of a short consensus motif called the KEN box (Pfleger & Kirschner, 2000; Pines, 2011). During S/$G_2$ phase, premature APC/C activation is at least in part prevented through CDK-mediated phosphorylation of Cdh1, which hinders association of Cdh1 with the APC/C (Lukas *et al*, 1999; Kramer *et al*, 2000; Miller *et al*, 2006).

As a first indication of APC/C$^{Cdh1}$ playing a role in the DDR, *CDH1*$^{-/-}$ chicken DT40 cells failed to maintain a $G_2$ arrest after IR (Sudo *et al*, 2001). In addition, activation of the APC/C$^{Cdh1}$ in response to DNA damage during $G_2$ phase was shown to depend on the Cdc14B phosphatase and to result in the degradation of Polo-like kinase 1 (Plk1) (Bassermann *et al*, 2008; Wiebusch & Hagemeier, 2010). Upon completion of DSB repair, Cdk1 and Plk1 are reactivated to allow cell cycle progression from $G_2$ into mitosis (van Vugt *et al*, 2004). Further experiments performed in Cdc14B-deficient cells showed that those cells are unable to repair DSBs even if they efficiently arrest in $G_2$ (Mocciaro *et al*, 2010). However, direct participation of the APC/C$^{Cdh1}$ in the regulation of DSB repair has never been reported. The observation that Cdh1-depleted cells or *Cdh1*$^{-/-}$ mice have elevated levels of DNA damage and chromosomal aberrations (García-Higuera *et al*, 2008; Sigl *et al*, 2009; Delgado-Esteban *et al*, 2013) strengthens this notion, but direct mechanistic insights into how the APC/C$^{Cdh1}$ ubiquitin ligase connects the cell cycle machinery to DNA repair is still lacking and the responsible substrates remain elusive.

In this study, we show that inactivation of Cdh1 results in genomic instability in different human cell lines. Moreover, Cdh1-depleted cells are hypersensitive toward DNA-damaging agents and display reduced Rad51 foci upon IR treatment. Making use of an integrated proteomics and bioinformatics approach, we identify the DNA-end resection factor CtIP as a novel substrate of the APC/C$^{Cdh1}$ E3 ubiquitin ligase. CtIP–Cdh1 interaction is mediated by an evolutionary conserved KEN box and is required for the downregulation of CtIP protein levels both after mitotic exit and in late S/$G_2$ in response to DNA damage. U2OS cells inducibly expressing a CtIP KEN box mutant exhibit increased DNA-end resection capacity, which correlates with a decrease in HR and hypersensitivity to PARP inhibition. Together, our data describe a novel regulatory role for the APC/C$^{Cdh1}$ in DNA repair, at least in part by limiting CtIP-dependent DNA-end resection activity in late S/$G_2$ phases of the cell cycle.

## Results

### Cdh1 depletion provokes DNA damage and hypersensitivity to DSB-inducing agents

To analyze the role of APC/C$^{Cdh1}$ in the maintenance of genome stability, we stably suppressed Cdh1 in non-transformed, immortalized human retina pigment epithelium (hTERT-RPE-1), HeLa cervical cancer, and MCF7 breast cancer cells using lentiviral shRNAs (Fig 1A). Sustained downregulation of Cdh1 over the course of 5 days resulted in approximately twofold increase of cells in $G_2$/M phase accompanied by elevated levels of γ-H2AX (Fig 1A–C). Also, Cdh1 depletion resulted in upregulation of p53 in RPE-1 and MCF7 cells (Fig 1A and Supplementary Fig S1). Combined, these results are indicative of DNA damage accumulation in Cdh1-depleted cells, even in the absence of genotoxic agents, which is in line with observations in other cell types (García-Higuera *et al*, 2008; Sigl *et al*, 2009; Delgado-Esteban *et al*, 2013; Eguren *et al*, 2013). We next analyzed the distribution of cells over the various mitotic stages to address whether the acquisition of DNA damage caused by Cdh1 downregulation translates into aberrant mitotic progression. While Cdh1 depletion in MCF7 cells did not significantly alter the distribution of the various mitotic phases, it gave rise to a higher frequency of bridging chromosomes in anaphase (Fig 1D). Such abnormal chromosome segregation events are frequently observed in cells that exhibit $G_2$/M checkpoint or DNA repair defects (French *et al*, 2006; Acilan *et al*, 2007; Chan *et al*, 2007; Laulier *et al*, 2011).

This prompted us to examine whether Cdh1 depletion leads to increased sensitivity to DNA-damaging agents. Clonogenic survival assays showed that Cdh1-depleted MCF7 cells are hypersensitive to IR (Fig 2A). Notably, the colonies of irradiated Cdh1-depleted cells were considerably smaller compared to control-depleted cells (Fig 2A). In line with these results, we found that shRNA-mediated depletion of Cdh1 reduced cell survival after treatment with doxorubicin, a chemotherapeutic compound inducing DSBs (Fig 2B).

We next examined whether DSB repair mechanisms are affected by Cdh1 depletion. Since cell cycle status significantly influences the mode of DSB repair, we made use of the FUCCI system which allows to specifically analyze S/$G_2$ cells without employing synchronization protocols (Supplementary Fig S2A) (Sakaue-Sawano *et al*, 2008). First, Cdh1 depletion did not affect IR-induced phosphorylation of KAP1 at S824, an early event in the DNA damage response (Fig 2C) (White *et al*, 2006; Ziv *et al*, 2006). Interestingly, however, Cdh1-depleted cells displayed significantly reduced numbers of Rad51 foci at both 2 and 5 h after irradiation, without affecting Rad51 levels (Fig 2C and D, and Supplementary Fig S2B). In contrast, 53BP1 foci numbers remained largely unaffected by the absence of Cdh1 (Fig 2D and Supplementary Fig S2C). Taken together, our results demonstrate that Cdh1 ensures genome stability, promotes survival under conditions of DNA damage, and influences the dynamics of IR-induced Rad51 foci formation, indicative of a regulatory function of Cdh1 in HR.

### Proteomic analysis of potential Cdh1 targets

We next set out to identify APC/C$^{Cdh1}$ substrates that contribute to the role of Cdh1 in maintaining genome stability. To select for potential candidates, we focused on two selection criteria. Firstly, we screened for proteins that are downregulated when APC/C$^{Cdh1}$ activity is turned on after mitotic exit using quantitative mass spectrometry. Secondly, we analyzed the primary amino acid sequence of each of those downregulated proteins for the presence of so-called D-boxes and KEN boxes, through which Cdh1 recruits targets to the APC/C (Pfleger *et al*, 2001; Liu *et al*, 2012). To identify proteins that are degraded during the mitosis-to-$G_1$ transition, we treated cells with nocodazole, a reversible microtubule-depolymerizing agent that activates the spindle assembly checkpoint, thereby causing cells to

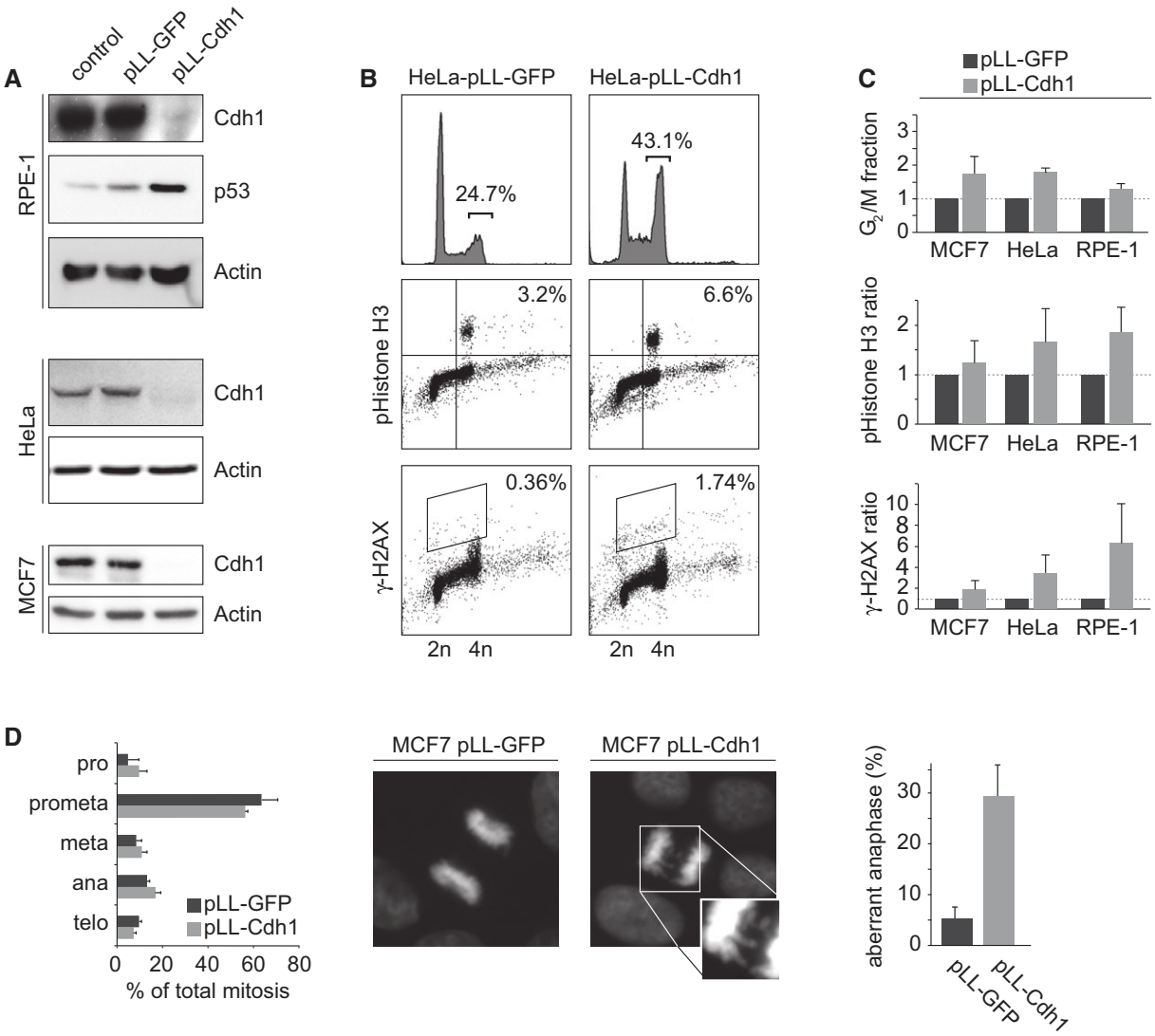


**Figure 1. Cdh1 depletion results in genomic instability.**

A RPE-1, HeLa, and MCF7 cells were infected with pLL-GFP or pLL-Cdh1 lentiviral shRNAs, and puromycin-resistant cells were harvested at 5 days after virus infection. Immunoblotting was performed with anti-Cdh1, anti-p53, and anti-actin antibodies.

B HeLa cells treated as in (A) were harvested in ice-cold ethanol and co-stained for γ-H2AX and phospho-histone H3 along with propidium iodide before analysis by flow cytometry. Plots of at least 10,000 events are shown. Percentages indicate average amounts of $G_2$/M cells, phospho-histone H3-positive cells, and γ-H2AX-positive cells.

C RPE-1, HeLa, and MCF7 cells were treated as in (B), and averages and standard deviations for three independent experiments are indicated for $G_2$/M content, phospho-histone H3-positive cells, and γ-H2AX-positive cells.

D MCF7 cells were infected with the indicated shRNA viruses, grown on glass coverslips and stained with DAPI. From three experiments, at least 200 mitoses were scored per condition. Anaphase figures were scored separately for the presence of lagging chromosomes. Averages and standard deviations are indicated. Representative examples are indicated.

arrest in prometaphase. Subsequent removal of nocodazole allows cells to synchronously exit mitosis along with APC/C$^{Cdh1}$ activation. To compare protein abundance before and after mitotic exit, RPE-1 cells were grown in DMEM containing either light or heavy isotope-labeled amino acids (Ong *et al*, 2002). Cells cultured in light medium were lysed directly after nocodazole incubation, whereas cells in heavy medium were harvested at 2.5 h after being released from mitotic arrest (Fig 3A and B). In addition, a label-swap experiment was performed with the SILAC labeling reversed. Cell lysates were then mixed in a 1:1 ratio and analyzed by mass spectrometry. We measured relative up- or downregulation of > 3,300 proteins in $G_1$ compared to M phase (Supplementary Data S1). To interrogate the quality of our data set, we assessed whether specific pathways were predominantly affected during mitotic exit. To this end, protein entries were converted to gene entries and enrichment was tested using Gene set enrichment analysis (GSEA) (Subramanian *et al*, 2005). As expected, "cell cycle" and "mitotic" pathways were significantly downregulated during mitotic exit (Fig 3C). In

 

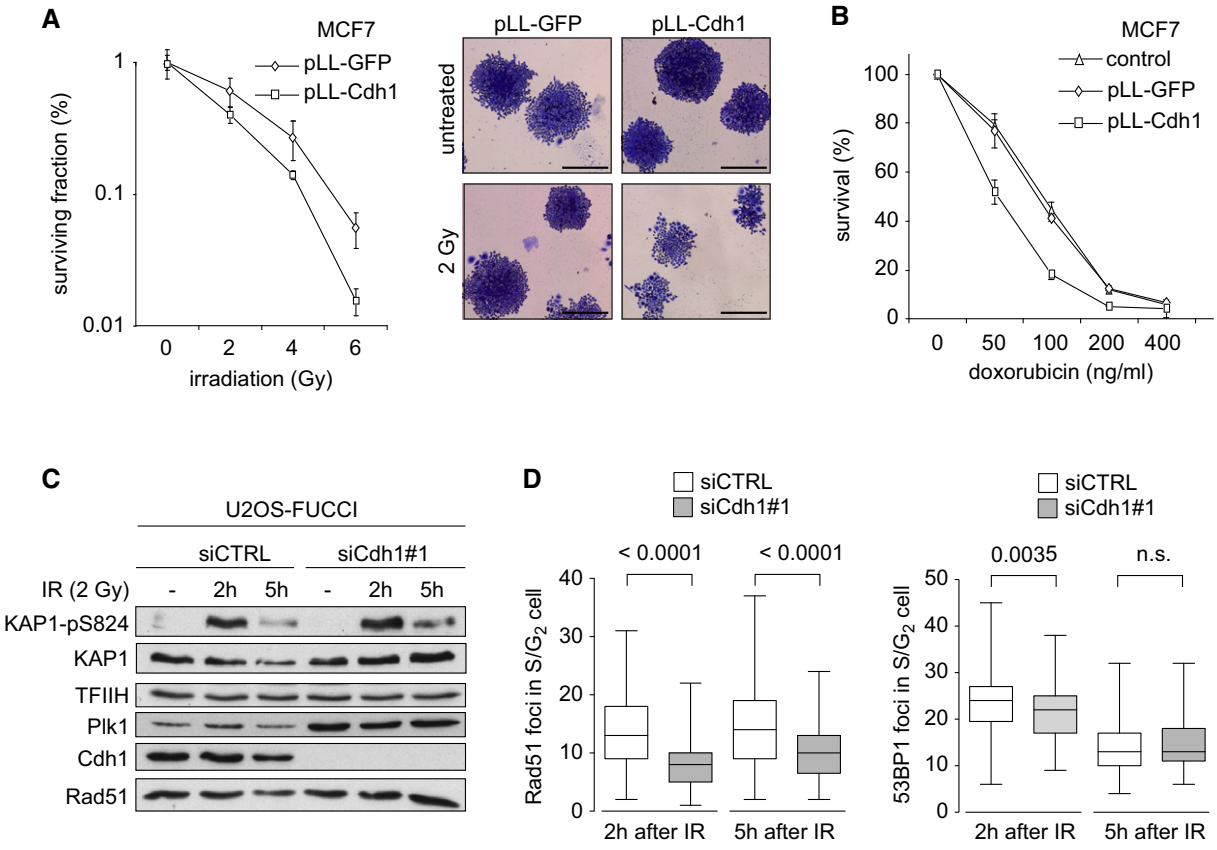


**Figure 2. Cdh1 depletion sensitizes to DNA-damaging agents and affects recruitment of DNA repair components.**

A MCF7 cells were infected with the indicated shRNAs and selected with puromycin. pLL-GFP- or pLL-Cdh1-infected MCF7 cells were plated in 6-well plates and subsequently irradiated with the indicated amounts of ionizing radiation. Surviving colonies were stained, and relative amounts of colony numbers compared to non-irradiated cells are shown. Averages and standard deviations of three independent experiments are shown.

B pLL-GFP- or pLL-Cdh1-infected MCF7 cells were plated in 96-well plates and subsequently treated with the indicated amounts of doxorubicine for 4 days. Cellular viability was assessed using MTT conversion, and untreated cells were used as a reference. Averages and standard deviations of three independent experiments are shown.

C At 48 h after siRNA transfection, U2OS-FUCCI cells were irradiated (2 Gy). At 2 or 5 h after treatment, whole-cell extracts were prepared and analyzed by Western blotting with the indicated antibodies.

D U2OS-FUCCI cells treated as in (C) were prepared for 53BP1 and Rad51 immunofluorescence. Graphs show the amounts of 53BP1 or Rad51 foci in S/$G_2$ cells. At least 120 cells from three independent experiments were counted for each condition, and data are presented as box plots with whiskers representing the minimal and maximal values. Unpaired Student's *t*-tests (two-sided) were done to compare control-depleted and Cdh1-depleted conditions. Representative images can be found in Supplementary Fig S2B and C.

contrast, proteins involved in translation and transcription were upregulated, in line with observations that chromatin is re-established after mitosis and that translational and transcriptional processes are inactive during mitosis and need to be re-initiated upon mitotic exit (Fig 3C) (Prescott & Bender, 1963; Bonneau & Sonenberg, 1987).

Our data set for proteins that were considerably downregulated after mitotic exit included various known APC/C$^{Cdh1}$ targets such as p15-PAF, cyclin B1, Plk1, UbcH10, Aurora A, and Aurora B (Fig 3D and Supplementary Fig S3A) (Pfleger *et al*, 2001; Littlepage & Ruderman, 2002; Taguchi *et al*, 2002; Lindon & Pines, 2004; Rape & Kirschner, 2004; Nguyen *et al*, 2005; Stewart & Fang, 2005; Emanuele *et al*, 2011). As expected, both KEN box and D-box motifs were significantly enriched in proteins downregulated during mitotic exit compared to the entire proteomic data set (Fig 3E) (Liu *et al*, 2012). When we applied "DNA damage response" (see Supplementary Table S1 for list of Gene Ontology terms) as a functional criterion for proteins downregulated during mitotic exit containing a conserved destruction motif, we discovered various proteins involved in the maintenance of genomic integrity including Rif1, Smc5, Mdc1, CtIP, and Top2A (Fig 3F). DNA topoisomerase 2-alpha was recently discovered as a novel Cdh1 substrate (Eguren *et al*, 2014). Interestingly, Rif1 has been reported to act as a 53BP1 effector protein, antagonizing the role of BRCA1 in promoting CtIP-dependent resection and HR (Kumar & Cheok, 2014). However, sequence analysis revealed that none of the predicted functional destruction motifs in human Rif1 were evolutionary conserved, whereas both putative KEN boxes in human CtIP were highly conserved in vertebrates (Supplementary Fig S3). Therefore, we decided to focus on the DNA-end resection factor CtIP as a potential target of the APC/C$^{Cdh1}$ involved in the maintenance of genomic integrity.

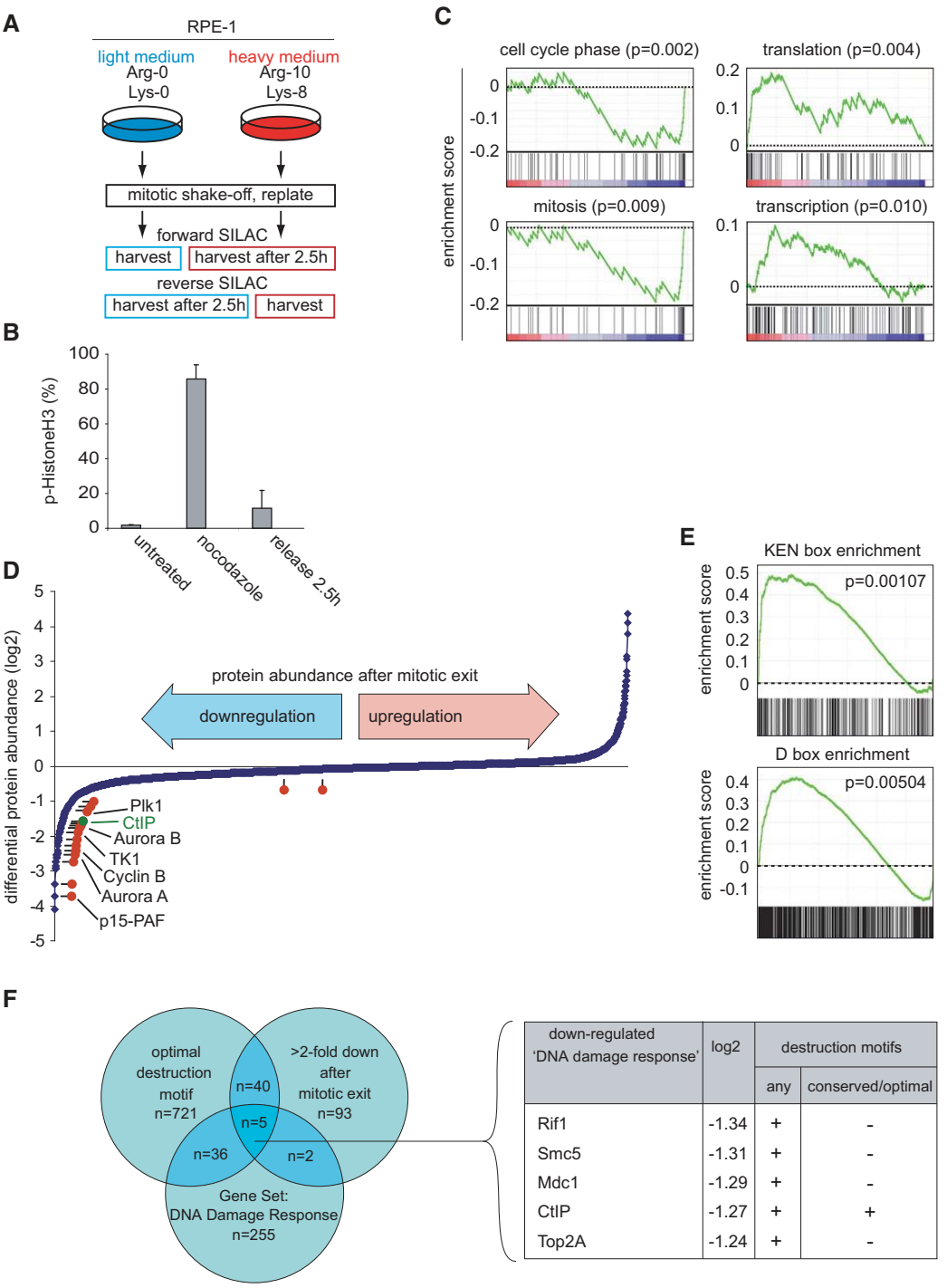


**Figure 3. A combined proteomics/bioinformatics approach to identify potential APC/C$^{Cdh1}$ substrates.**

A Overview of mass spectrometry analysis of changes in protein abundance during mitotic exit. RPE-1 cells were grown in "light" or "heavy" SILAC media and treated with nocodazole. Mitotic cells were obtained by shake-off and were directly lysed or replated in nocodazole-free medium and lysed after 2.5 h. Alternatively, treatments were swapped ("reverse SILAC"). Cell lysates were mixed 1:1 and analyzed by mass spectrometry.

B RPE-1 cells were treated and harvested in parallel to (A) and were stained for phospho-histone H3/Alexa-488.

C Gene set enrichment analysis (GSEA) of SILAC results. Indicated pathways are significantly affected during mitotic exit.

D Log2-transformed ratios are indicated for the > 3,300 proteins that were identified both in forward and in reverse SILAC. Negative ratios indicate downregulation during mitotic exit. Established APC/C$^{Cdh1}$ targets are indicated in red.

E GPS-ARM software was used to identify D-box or KEN box sequences in mass spectrometry hits. GSEA was used to assess enrichment for destruction motif-containing proteins within downregulated proteins.

F Venn diagram indicating proteins that are downregulated at least twofold, contain any destruction motif, and belong to the "DNA damage response/DNA repair" gene set.

### CtIP is a substrate of APC/C$^{Cdh1}$ during mitotic exit

Confirming our mass spectrometry data, we observed that CtIP protein levels decreased when RPE-1 cells exit mitosis following release from a nocodazole-induced prometaphase arrest (Fig 4A–C). Notably, CtIP downregulation followed a pattern similar to that of Plk1, a known APC/C$^{Cdh1}$ substrate (Fig 4A–C) (Lindon & Pines, 2004). This was not due to nocodazole-induced microtubule depolymerization, as cells released from a mitotic block induced by Eg5 inhibition showed a similar behavior with regard to CtIP levels (Supplementary Fig S4A). Likewise, when cells were enriched at the $G_2$/M transition using the reversible Cdk1 inhibitor RO-3306, and subsequently followed during exit from mitosis, we observed that CtIP protein levels gradually decreased (Fig 4D). Interestingly, under these different synchronization conditions, we repeatedly noticed that CtIP migrates much slower in mitotic cells compared to $G_1$ cells. We find that this shift is mainly attributed to phosphorylation, but further work is needed to explore whether there is a functional interplay between CtIP phosphorylation and stability during exit from mitosis (Supplementary Fig S4B).

In line with the APC/C$^{Cdh1}$ targeting CtIP for proteasomal degradation, we observed increased CtIP protein levels after transfecting RPE-1 and U2OS cells with Cdh1 siRNA oligos (Fig 4E and Supplementary Fig S4C and D), which was not due to altered cell cycle distribution profiles (Supplementary Fig S4C and D). Analogously, treatment of asynchronously growing RPE-1 cells with the small molecule APC/C inhibitor proTAME (Zeng *et al*, 2010) stabilized CtIP as well as Plk1, albeit not to the same extent as treatment with the proteasome inhibitor MG-132 (Fig 4F). Importantly, both MG-132 and proTAME clearly blocked CtIP and Plk1 degradation after cells synchronously exit mitosis and enter $G_1$ phase (Fig 4G and Supplementary Fig S4E). Taken together, our findings indicate that CtIP is targeted by APC/C$^{Cdh1}$ during mitotic exit.

### CtIP interacts with Cdh1 through a conserved KEN box

CtIP contains two conserved KEN box motifs, which are believed to be recognized exclusively by APC/C$^{Cdh1}$ (Pfleger & Kirschner, 2000), but only the second one between amino acids 467 and 469 matches the recently reported consensus KEN box sequence ([D/N]-K-E-N-x-x-P) (Fig 5A) (He *et al*, 2013). To test whether any of the two KEN box motifs are functional, HEK293T cells were transfected with HA-Cdh1, along with FLAG-CtIP mutated in one or both KEN box motifs. Whereas CtIP-wt and CtIP-K179A are efficiently co-immunoprecipitated with HA-Cdh1, mutating the second putative KEN box in CtIP (K467A) abolished its interaction with Cdh1 (Fig 5B). Furthermore, only GFP-CtIP-wt, but not GFP-CtIP-K467A, was efficiently co-immunoprecipitated with endogenous Cdh1 (Supplementary Fig S5A). To strengthen these observations, we subjected HeLa nuclear extracts to GST-CtIP pull-down assays and found that endogenous Cdh1 interacts with wild-type recombinant CtIP, but not with the CtIP-K467A mutant (Fig 5C). Moreover, this was unlikely due to improper protein folding of bacterially expressed GST-CtIP-K467A, as the mutant full-length protein was still able to pull-down Mre11 (Fig 5C). These results were confirmed using a CtIP fragment covering both KEN box motifs (166–487), indicating that the coiled coil domain (45–160) and the conserved Sae2-like C-terminal domain (790–897) of CtIP are not required for Cdh1 interaction (Fig 5A and C).

The APC/C is a multi-subunit E3 ubiquitin ligase that, once activated by either Cdc20 or Cdh1, mediates ubiquitin- and proteasome-dependent degradation of key cell cycle regulatory proteins (Peters, 2006). Since CtIP was recently shown to be poly-ubiquitylated and degraded by the proteasome (Steger *et al*, 2013), we next addressed whether Cdh1 may promote CtIP ubiquitylation. To this end, we transfected His-ubiquitin into HEK293 cells inducibly expressing GFP-CtIP and analyzed the level of CtIP ubiquitylation after Ni-NTA pull-down. Remarkably, depletion of Cdh1 using two independent siRNAs severely impaired CtIP ubiquitylation (Fig 5D). Furthermore, the conjugation of ubiquitin chains was largely abolished in the CtIP-K467A KEN box mutant compared to CtIP-wt, further indicating that CtIP is a substrate of APC/C$^{Cdh1}$ (Fig 5E). To test whether the conserved KEN box is required for CtIP degradation during mitotic exit, we performed time-lapse fluorescence microscopy with U2OS cells harboring siRNA-resistant inducible GFP-tagged CtIP-wt or CtIP-K467A (Fig 5F). These cell lines progressed through the cell cycle with similar kinetics and expressed comparable levels of GFP-tagged CtIP upon doxycycline addition (Supplementary Fig S5B). Importantly, whereas the fluorescence intensity of nuclear CtIP-wt slowly decreased after exit from mitosis, CtIP-K467A levels remained relatively constant throughout the entire time course (Fig 5F). Combined, our data suggest that CtIP interacts with Cdh1 through a conserved KEN box motif and this interaction promotes CtIP poly-ubiquitylation and degradation in an APC/C$^{Cdh1}$-dependent manner.

**Figure 4. CtIP is a substrate of the APC/C$^{Cdh1}$ during mitotic exit.**

A RPE-1 cells were left untreated (asynchronous, "AS") or treated with nocodazole for 16 h. Mitotic cells were obtained by shake-off and replated in nocodazole-free medium for indicated time periods. Cells were stained for phospho-histone H3 and propidium iodide, and at least 10,000 events were analyzed by flow cytometry. Averages and standard deviations of three experiments are shown.

B Same cells as in (A) were immunoblotted for the indicated proteins.

C Western blots as shown in (B) were quantified, and averages and standard deviations of three independent experiments are shown.

D RPE-1 cells were treated for 18 h with the Cdk1 inhibitor RO-3306 (5 μM) to enrich for $G_2$ cells. Subsequently, cells were washed 3 times with warm culture medium, and 1 h later, mitotic cells were collected by mitotic shake-off ($t$ = 0 h). At the indicated time points after replating, cells were harvested and further analyzed as in (A) and (B).

E Asynchronously growing RPE-1 cells were transfected with indicated siRNAs for 48 h and processed for immunoblotting with the indicated antibodies. Western blots were quantified, and averages and standard deviations of three independent experiments are shown.

F RPE-1 cells were cultured for 3 h in proTAME (12 μM), MG-132 (5 μM), or solvent controls. Whole-cell lysates were immunoblotted for the indicated proteins (left panel). Average Western blot intensities and standard deviations of three independent experiments are shown (right panel).

G Mitotic RPE-1 cells were obtained by mitotic shake-off after nocodazole treatment. Cells were replated, and after 1 h, proTAME (12 μM) or MG-132 (5 μM) or solvent was added to the culture medium. At 1 or 2.5 h after treatment, cells were harvested for Western blot analysis with the indicated antibodies. Western blots of a representative experiment are indicated (left panel). In parallel, cells were fixed in ethanol and stained for phospho-histone H3 and propidium iodide, and at least 10,000 events were analyzed by flow cytometry. Averages and standard deviations of three independent experiments are shown (right panel).

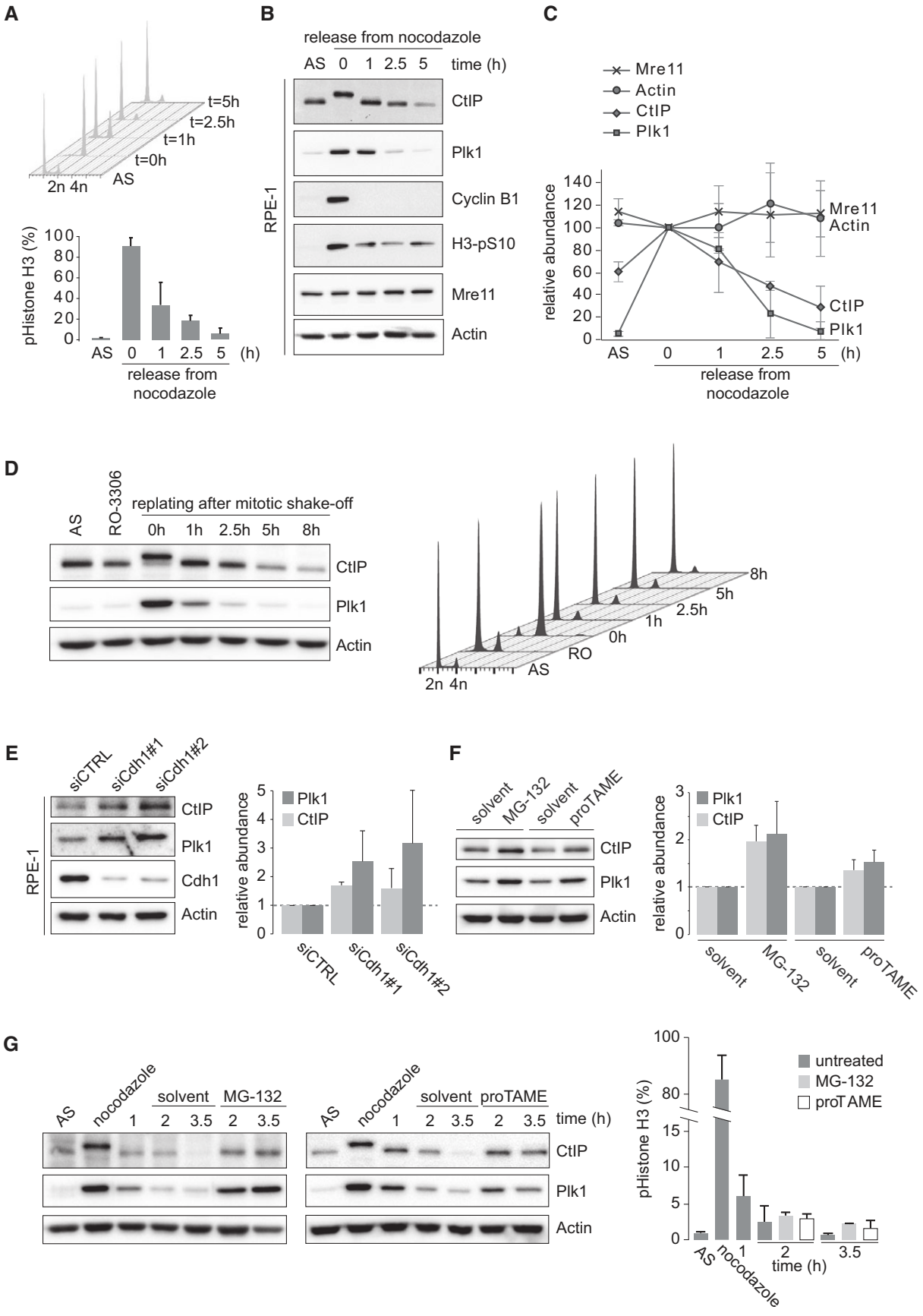


**Figure 4.**

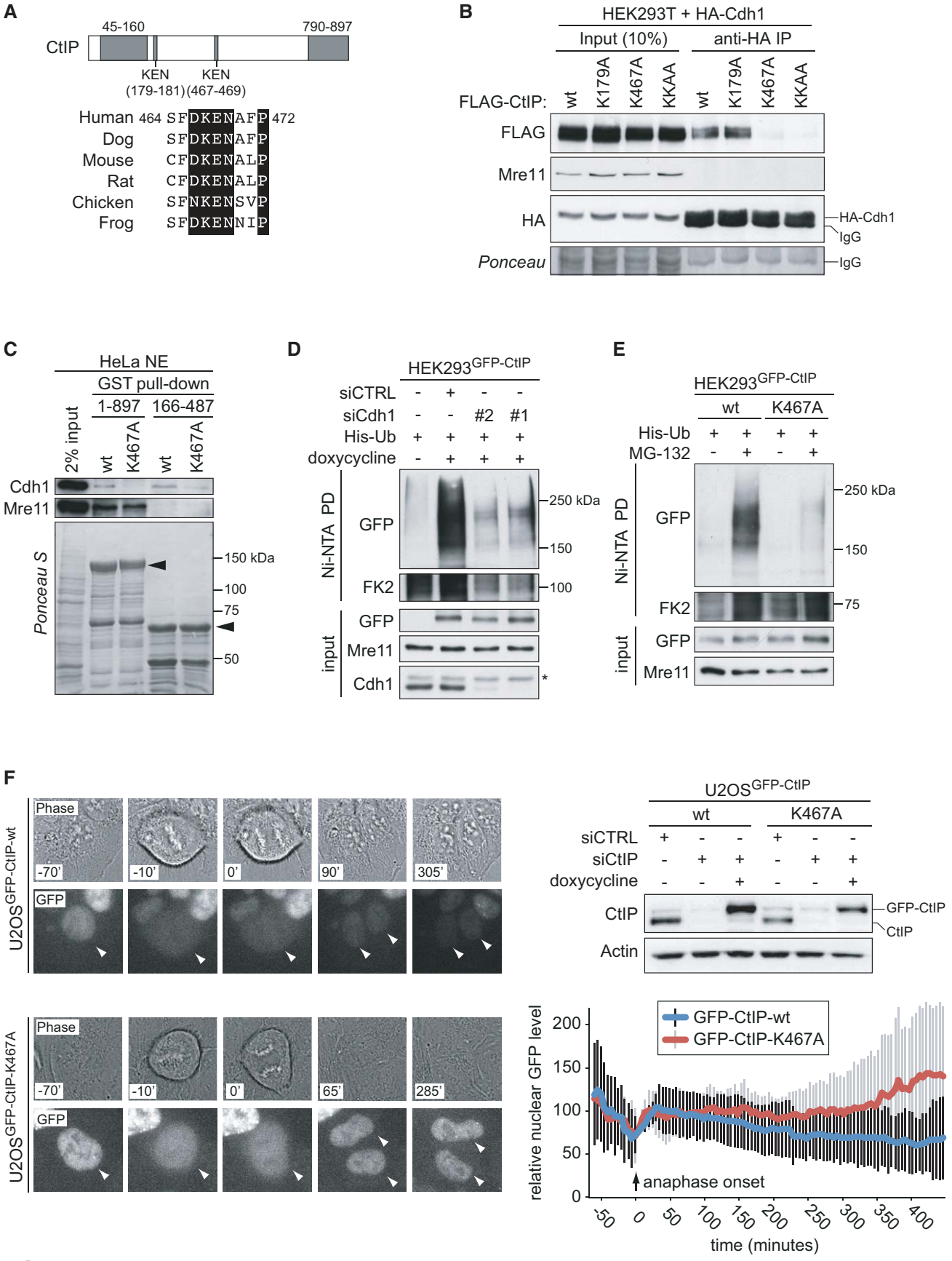


**Figure 5.**

### APC/C promotes CtIP degradation in response to DSBs

Since APC/C$^{Cdh1}$ has been described to be activated in $G_2$ phase after DNA damage (Sudo *et al*, 2001; Bassermann *et al*, 2008), we decided to investigate whether CtIP is also targeted by the APC/C under these conditions. To this end, we synchronized U2OS cells at the $G_1$/S transition using a single thymidine treatment and then allowed cells to re-enter the cell cycle. At 7 h after the release, $G_2$-enriched cells were irradiated at low (2 Gy) or high dose (10 Gy) and analyzed after 2 and 5 h by Western blotting (Fig 6A). Whereas CtIP levels only slightly decreased at 5 h after 2 Gy, CtIP downregulation in response to 10 Gy occurred to an extent that was similar to that of Claspin, a previously reported APC/C$^{Cdh1}$ substrate (Fig 6B) (Bassermann *et al*, 2008). These changes did not represent post-mitotic degradation of CtIP, as judged by comparable cell cycle profiles (Fig 6A). Importantly, CtIP and Claspin levels were partially restored when proTAME was added to the cells immediately after IR (Fig 6B), indicating that the APC/C is responsible for CtIP degradation in $G_2$-irradiated cells. Similar results were obtained after treatment of $G_2$-enriched cells with doxorubicin (Supplementary Fig S6A and B). Interestingly, we noticed that proTAME treatment led to an increase in RPA2 phosphorylation following IR (Fig 6B, lane 7), while other DNA damage signaling events including Chk1 and Chk2 phosphorylation remained largely unaffected. In line with a requirement for the APC/C in CtIP degradation after DNA damage in $G_2$ cells, ubiquitylation of endogenous CtIP in response to IR was significantly reduced in presence of proTAME (Fig 6C).

To strengthen these findings, we monitored GFP-CtIP-wt fluorescent intensity following irradiation of $G_2$ cells using live-cell imaging. Consistent with our Western blot data, CtIP levels drop to approximately 50% starting at 4 h after IR (Fig 6D and Supplementary Fig S6C). Also in this case, the observed CtIP downregulation was not due to post-mitotic degradation, since none of the analyzed cells entered mitosis during the entire time-lapse experiments, most likely due to a strong $G_2$-arrest produced by 10 Gy (data not shown). In line with our previous observation, GFP-CtIP-wt levels in cells co-treated with proTAME remained constant throughout the analyzed time frame, supporting our hypothesis that the APC/C is required for CtIP downregulation in response to DNA damage in $G_2$ cells (Fig 6D and Supplementary Fig S6C). Altogether, these data suggest that CtIP is degraded after DSB induction in $G_2$ and that this regulatory mechanism is dependent on APC/C activity.

### CtIP–Cdh1 interaction is required for CtIP downregulation after DNA damage and clearance of IR-induced CtIP foci

Having established that CtIP is degraded in an APC/C-dependent manner in response to DNA damage, we wanted to test whether this requires physical interaction between Cdh1 and CtIP. Quantitative live-cell imaging revealed that a functional KEN box is crucial for IR-induced downregulation of CtIP, since GFP-CtIP-K467A levels remained stable throughout the entire time course (Fig 7A and B). Strikingly, we observed that CtIP-K467A IR-induced foci (IRIF) persisted, whereas CtIP-wt IRIF were resolved over time, indicating that APC/C$^{Cdh1}$ facilitates the spatiotemporal release of CtIP from damaged chromatin (Fig 7C). Analysis of GFP-CtIP localization in response to laser micro-irradiation further confirmed that both CtIP-wt and CtIP-K467A are efficiently recruited to microlaser-generated DSB tracks, and overlap with γ-H2AX-decorated chromatin (Supplementary Fig S7A).

To further investigate the role of Cdh1–CtIP interaction in response to DNA damage, we isolated monoclonal cell lines, inducibly expressing siRNA-resistant GFP-CtIP-wt and GFP-CtIP-K467A. Importantly, expression of GFP-CtIP-wt rescued DNA-end resection defects caused by CtIP depletion, as judged by the restoration of RPA2 phosphorylation at S4/S8 in response to IR treatment (Supplementary Fig S7B) (Sartori *et al*, 2007). The DNA-end resection capacity of CtIP was previously shown to be required for the maintenance of IR-induced $G_2$ arrest (Kousholt *et al*, 2012). In line with this report, depletion of CtIP did not interfere with checkpoint initiation, but did result in defective checkpoint maintenance (Supplementary Fig S7C). Notably, expression of either GFP-CtIP-wt or GFP-CtIP-K467A rescued the checkpoint maintenance defect (Supplementary Fig S7C), suggesting that CtIP-K467A is proficient in DNA-end resection. In addition, we did not find any significant defects in initiation and maintenance of the IR-induced $G_2$ checkpoint upon Cdh1 depletion (Supplementary Fig S7D).

In agreement with CtIP-K467A mutant cells being checkpoint proficient, irradiation resulted in robust activation of ATM and ATR, as assessed by Chk2 and Chk1 phosphorylation, respectively (Fig 7D). Moreover, both CtIP-wt and CtIP-K467A were able to promote RPA2 phosphorylation, with the KEN box mutant being slightly more efficient than the wt, whereas expression of the resection-deficient CtIP-T847A mutant largely

**Figure 5. CtIP interacts with Cdh1 through a conserved KEN box.**

A Schematic representation of human CtIP protein with its coil-coiled domain (45–160), Sae2-like domain (790–897), and putative KEN boxes (179–181 and 467–469). Conservation of KEN box at 467 is shown for the indicated species.

B HEK293T cells were transfected with HA-Cdh1 in combination with indicated FLAG-CtIP plasmids. Cells lysates were used for anti-HA immunoprecipitations. Western blotting was performed with the indicated antibodies for whole-cell lysate or immunoprecipitations.

C HeLa nuclear extract (NE) was incubated with GST fusion proteins with the indicated full-length (1–897) CtIP variants or CtIP fragment (166–487) variants. GST pull-downs were immunoblotted for Mre11 and Cdh1.

D HEK293 Flp-In T-REx cells were induced to express GFP-CtIP-wt using doxycycline and were transfected with His-tagged ubiquitin ("His-Ub") along with control siRNA or Cdh1 siRNA. Before lysis, cells were treated with proteasome inhibitor MG-132 for 4 h. Cell lysates were used for Ni-NTA precipitations. Total cell lysates ("input") and Ni-NTA pull-downs ("PD") were immunoblotted for the indicated proteins.

E HEK293 Flp-In T-REx cells were induced to express GFP-CtIP-wt or GFP-CtIP-K467A and transfected with His-tagged ubiquitin ("His-Ub"), and treated with proteasome inhibitor MG-132 for 4 h. Cell lysates were subsequently used for Ni-NTA pull-down. Total cell lysates ("input") and Ni-NTA pull-downs ("PD") were immunoblotted for the indicated proteins.

F U2OS Flp-In T-REx cells were induced to express GFP-CtIP-wt or GFP-CtIP-K467A and were transfected with control siRNA or siCtIP. Cell lysates were processed for immunoblotting for CtIP and actin (upper right panel). U2OS cells were then imaged every 5 min for GFP expression or phase contrast using live-cell microscopy. Representative stills from live-cell imaging are shown, in which anaphase onset was used as a reference time point (left panels). Quantifications of the average nuclear GFP signal from time-lapse movies are indicated for GFP-CtIP-wt ($n$ = 12) and GFP-CtIP-K467A ($n$ = 18) (lower right panel).

 

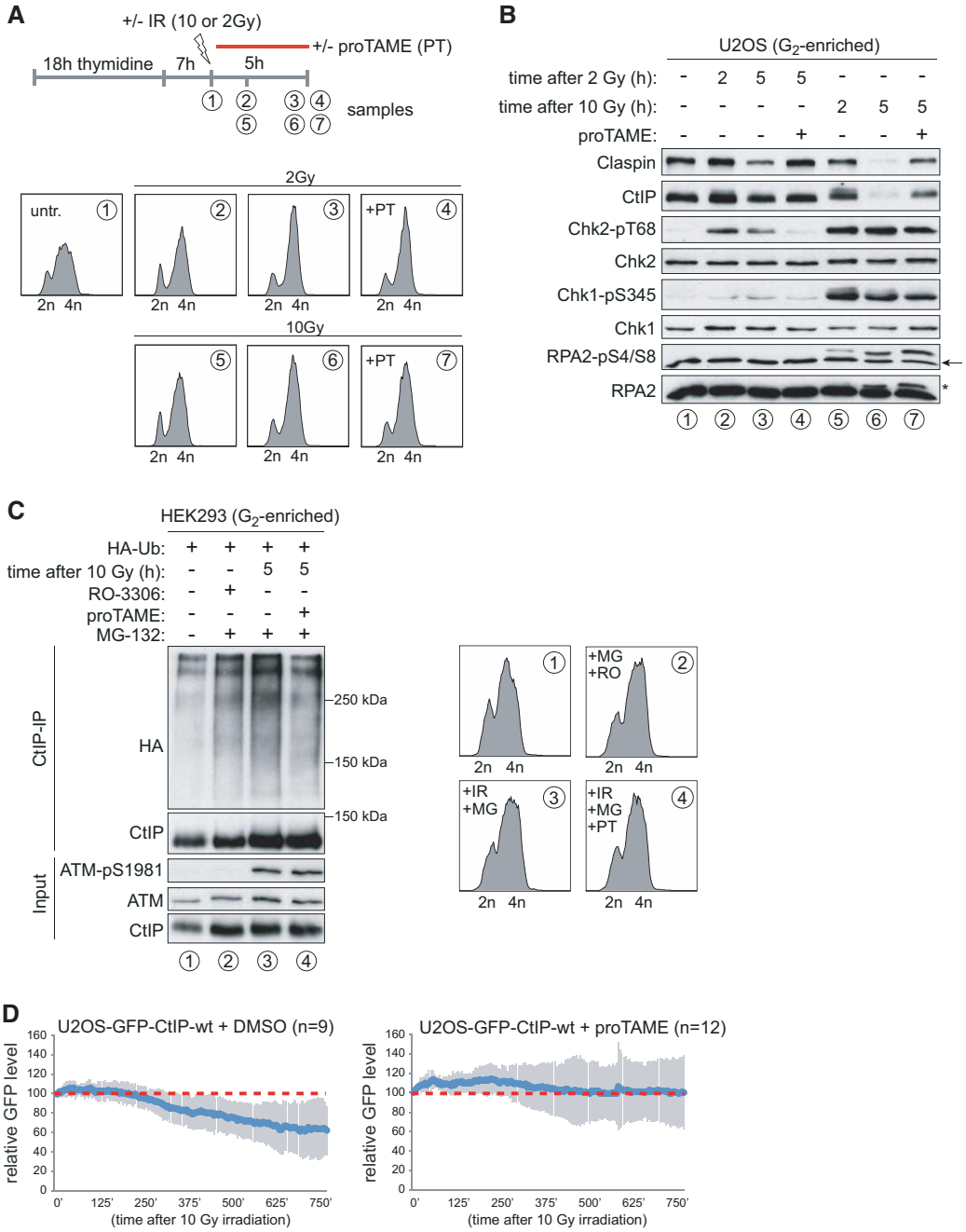


**Figure 6. CtIP is degraded in response to DNA damage in $G_2$ phase in an APC/C-dependent manner.**

A U2OS cells were synchronized using a single thymidine block with 2 mM thymidine for 18 h. Seven hours after release, cells enriched in $G_2$ phase were either fixed directly (lane 1) or exposed to low (2 Gy) or high dose (10 Gy) of IR and harvested at the indicated time points following irradiation. Where indicated, cells were treated with the APC inhibitor proTAME (20 μM) immediately after irradiation. Cells were stained with DAPI and analyzed by flow cytometry.

B Cells were treated as in (A) and lysed in RIPA buffer for immunoblotting with the indicated antibodies. The anti-RPA2 blot was reprobed with anti-pRPA2-S4/S8 antibody. The arrow indicates leftover signals of the unmodified RPA2 protein. The asterisk indicates hyperphosphorylated RPA2.

C HEK293 cells were transfected with HA-tagged ubiquitin ("HA-Ub"). Thirty hours post-transfection, cells were synchronized using a single thymidine block with 2 mM thymidine for 18 h. Five hours after the release, cells enriched in late S/$G_2$ phase were either lysed directly (lane 1), or further incubated for 5 h in the presence of CDK1 inhibitor RO-3306 (9 μM) to keep cells in $G_2$ (lane 2), or irradiated with 10 Gy in the absence (lane 3) or presence (lane 4) of the APC inhibitor proTAME (20 μM) and lysed after 5 h. Where indicated, cells were treated with MG-132 (20 μM) for 5 h before lysis. Samples were then further processed for immunoprecipitation using a polyclonal anti-CtIP antibody as indicated in Materials and Methods. Cell cycle profiles of corresponding samples are indicated on the right.

D U2OS Flp-In T-REx cells were induced to express GFP-CtIP-wt and transfected with CtIP siRNA. Cells were subsequently synchronized by thymidine incubation for 24 h and released from thymidine for 8 h. At 8 h after release, cells were treated with DMSO or proTAME (12 μM), subsequently irradiated with 10 Gy, and imaged using fluorescence time-lapse microscopy. Representative stills of GFP and DIC movies are presented in Supplementary Fig S6C. Averages and standard deviations of total nuclear GFP intensity are indicated from 9 and 12 movies for DMSO-treated and proTAME-treated cells, respectively.

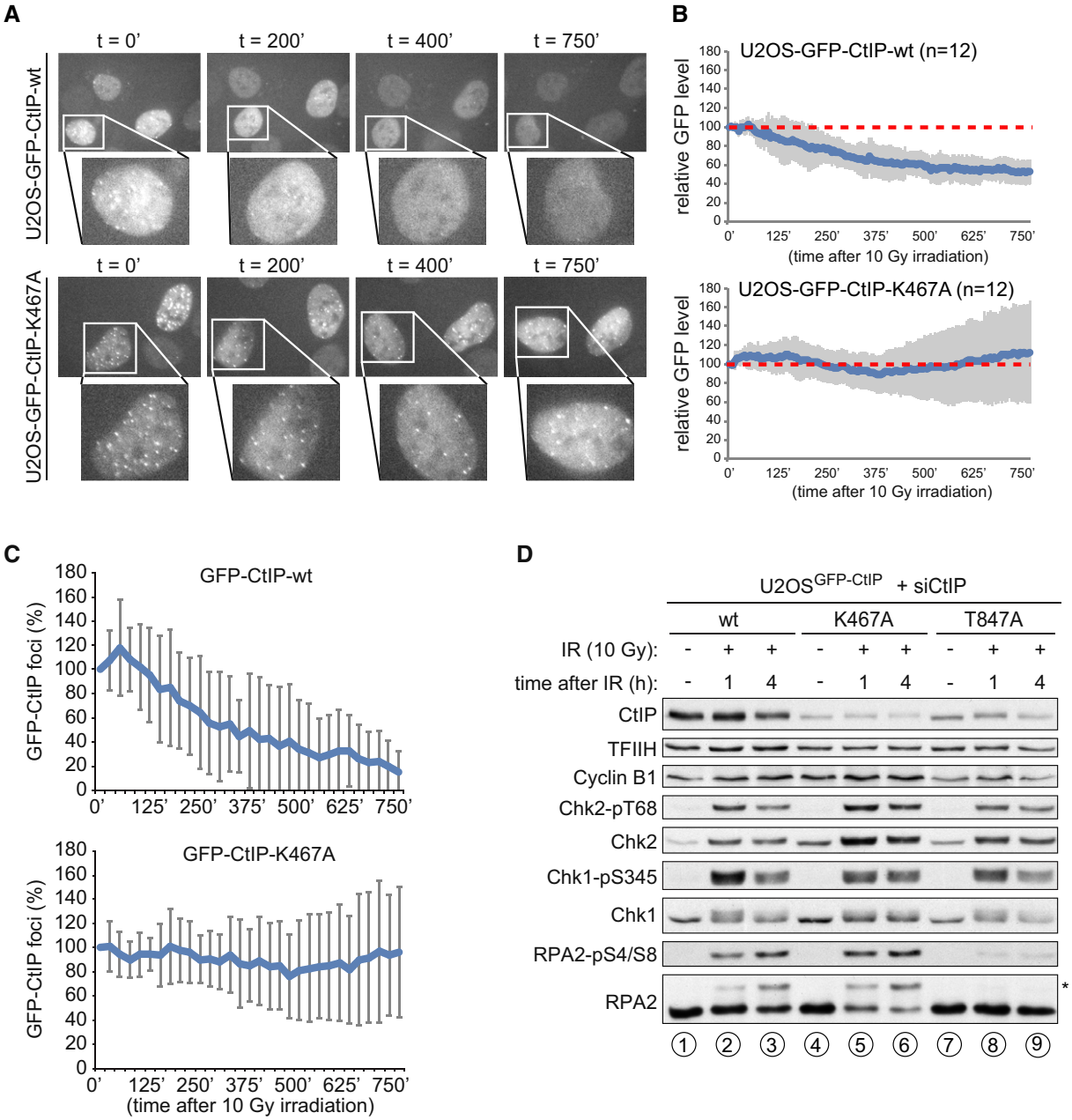


**Figure 7. CtIP–Cdh1 interaction is not required for CtIP recruitment to sites of DNA damage and initiation of DNA-end resection.**

A U2OS Flp-In T-REx cells were induced to express GFP-CtIP-wt or GFP-CtIP-K467A and transfected with CtIP siRNA. Cells were subsequently synchronized by thymidine incubation for 24 h and released for 8 h. GFP-CtIP-wt and GFP-CtIP-K467A were expressed to similar degree, and expression of GFP-CtIP-wt or GFP-CtIP-K467A did not alter cell cycle progression as judged by flow cytometry (Supplementary Fig S5B). Cells were then irradiated with 10 Gy and imaged using fluorescence time-lapse microscopy. Representative stills are indicated for GFP and DIC images.

B Quantifications of time-lapse movies from (A). Averages and standard deviations of total nuclear GFP intensity are indicated from 12 movies for each cell line.

C In the same experiment as described in (A), numbers of GFP-CtIP foci per nucleus were counted and plotted as a percentage of GFP-CtIP foci at the start of imaging. Averages and standard deviations of 15 movies per cell line are indicated.

D U2OS Flp-In T-REx clones stably expressing doxycycline-inducible GFP-CtIP-wt, GFP-CtIP-T847A, and GFP-CtIP-K467A were transfected with siCtIP. At 24 h post-transfection, cells were cultivated in the absence or presence of doxycycline. At 48 h post-transfection, cells were mock-treated or harvested at the indicated time points following irradiation (10 Gy). Whole-cell lysates were immunoblotted using the indicated antibodies.

abolished RPA2 phosphorylation (Fig 7D) (Huertas & Jackson, 2009). These data suggest that CtIP–Cdh1 interaction is not required for DNA-end resection, but may control the proper timing of resection.

### The CtIP–Cdh1 interaction facilitates homology-directed repair

The above findings prompted us to test whether CtIP–Cdh1 interaction plays a role in DSB repair. To this end, we analyzed the repair

 

of I-*Sce*I-induced DSBs in HEK293 cell lines containing two different reporters measuring HR (DR-GFP) and total NHEJ (EJ5-GFP). As shown previously, CtIP depletion interfered with HR, and led to a slight increase in total NHEJ (Fig 8A and B) (Bennardo *et al*, 2008). Importantly, these effects could be rescued by expression of siRNA-resistant FLAG-CtIP-wt (Fig 8A and B). Interestingly, expression of the K467A mutant did not rescue HR, but caused a similar decrease as compared to the DNA-end resection-defective T847A mutant (Fig 8A and B). Surprisingly, unlike T847A, we observed that expression of K467A does not lead to a significant increase in total NHEJ (Fig 8C). The observation that CtIP-K467A impaired homology-directed repair but does not result in compensation through NHEJ, suggested a dominant negative effect of the KEN box mutant. To test this hypothesis, FLAG-CtIP constructs were transfected into HEK293 DR-GFP cells without siRNA-mediated depletion of endogenous CtIP. Indeed, expression of CtIP-K467A caused a reduction in HR, whereas expression of CtIP-wt or CtIP-T847A did not significantly alter HR (Fig 8D). Taken together, these results suggest that abolishing the interaction between CtIP and Cdh1 does not interfere with the initiation of DNA-end resection, which would otherwise increase NHEJ efficiency. Instead, after resection has been initiated, the CtIP–Cdh1 interaction appears to be required for the proper execution of downstream HR events.

Defective HR was previously shown to result in increased sensitivity to PARP inhibition (Bryant *et al*, 2005; Farmer *et al*, 2005). In line with a defect in HR, we observed that cells inducibly expressing GFP-CtIP-K467A showed elevated sensitivity to the PARP inhibitor olaparib, although not as pronounced as in GFP-CtIP-T847A mutant cells (Fig 8E). Notably, depletion of Cdh1 also resulted in an elevated sensitivity to PARP inhibition (Fig 8E). However, GFP-CtIP-K467A-expressing cells did not display hypersensitivity to IR or doxorubicin treatment, indicating that the inability of Cdh1 to interact with CtIP cannot explain all phenotypic responses associated with Cdh1 loss in combination with DNA damage (Supplementary Fig S8A–C).

Besides decreased DNA-end resection capacity, also excessive or temporally unrestricted resection may potentially impair HR. Since we have observed that CtIP is targeted by the APC/C for proteasomal degradation after DNA damage in $G_2$, we monitored DNA-end resection in wt and K467A mutant cells that had been synchronized in $G_2$ prior to IR (Fig 8F and Supplementary Fig S8D). Clearly, expression of GFP-CtIP-K467A resulted in elevated levels of RPA2 phosphorylation at S4/S8, indicative of hyper-resection. This matched our earlier observation of elevated levels of RPA2 phosphorylation upon proTAME treatment in irradiated cells (Fig 6B). Remarkably, increased RPA2 phosphorylation in GFP-CtIP-K467A-expressing cells coincided with lower amounts of Rad51 being recruited to damaged chromatin (Fig 8F). Combined, these data suggest that CtIP–Cdh1 interaction is involved in limiting DSB resection, which probably allows correct assembly of Rad51–ssDNA nucleoprotein filaments, to facilitate HR.

## Discussion

The response to DSBs is tightly regulated during the cell cycle. As a consequence, deregulated cell cycle control may lead to aberrant DSB repair and ensuing genomic instability. An example thereof is provided by the APC/C$^{Cdh1}$ cell cycle regulator, as genetic inactivation of Cdh1 in either mouse embryonic fibroblasts or primary human cells has been shown to cause elevated levels of DNA damage and chromosomal instability. We could recapitulate these findings in Cdh1-depleted human cell lines of different origins. Moreover, we were able to extend these findings and demonstrate that depletion of Cdh1 results in hypersensitivity to DSB-inducing agents and negatively affects Rad51 IRIF formation. Concerning potential APC/C substrates responsible for these effects, Rhp54 (the fission yeast ortholog of Rad54) and Rad17 were shown to be degraded by the APC/C (Trickey *et al*, 2008; Zhang *et al*, 2010). However, when Rad54 was investigated in other species, no APC/C-dependent degradation was observed, and the degradation of Rad17 by the APC/C appeared to be UV-induced and appeared to control checkpoint duration rather than DNA repair. Finally, Cdh1 was reported to control the duration of the $G_2$ cell cycle arrest in response to DSBs by targeting Polo-like kinase 1 (Plk1) for proteolytic degradation (Wäsch & Engelbert, 2005; Bassermann *et al*, 2008; Engelbert *et al*, 2008). So far, it remained elusive, however, whether the APC/C$^{Cdh1}$ also contributes to the regulation of DSB repair.

Using a proteomics analysis of mitotic exit combined with bioinformatics analysis of the presence of KEN and D-box motifs, we have identified a number of candidate APC/C$^{Cdh1}$ substrates. Several of the putative Cdh1 targets play key roles in the regulation of DSB repair, including Rif1, MDC1, SMC5, and CtIP. Detailed *in silico* analysis of multiple protein sequences for the conservation of putative KEN and D-box motifs guided us to focus on CtIP as a previously unrecognized APC/C$^{Cdh1}$ substrate. Human CtIP contains two conserved KEN box motifs, but only the second KEN box strongly matches the consensus sequence recently proposed by Barford and colleagues (He *et al*, 2013) and is required for Cdh1–CtIP interaction. In addition to being targeted by the APC/C$^{Cdh1}$ for proteasomal degradation in $G_1$, we discovered that CtIP protein levels are controlled by the APC/C$^{Cdh1}$ prior to mitotic entry in response to DSBs. Concerning the activation of the APC/C$^{Cdh1}$ in response to DNA damage in $G_2$ cells, we noted that APC/C$^{Cdh1}$ activation is achieved most efficiently after high levels of DNA damage. This implies that especially under conditions provoking high amounts of DNA damage, such as after chemotherapy or radiotherapy, the APC/C$^{Cdh1}$ may acquire new functions, which under these circumstances may determine cell fate and genomic integrity.

Due to its crucial role in initiating DNA-end resection, CtIP is essential for homology-directed repair of DSBs (Sartori *et al*, 2007; Bennardo *et al*, 2008). DNA-end resection dictates the choice between HR and NHEJ and is thus proposed to be tightly regulated during the cell cycle (Ferretti *et al*, 2013). For instance, CtIP phosphorylation at T847 by cyclin-dependent kinases represents a key step toward the commencement of DNA-end resection and, consequently, a CtIP-T847A mutant abrogates HR (Huertas & Jackson, 2009). Here, we show that a CtIP KEN box mutant (K467A) compromises HR to a similar extent as the T847A mutant, indicating that the interaction between Cdh1 and CtIP facilitates HR. NHEJ requires only very limited DSB processing and is therefore not suitable for repairing DSBs which have undergone extensive resection. In other words, NHEJ can only compensate for HR in cells that are defective in DNA-end resection (Shibata *et al*, 2011). This is in line with our results showing that CtIP-T847A results in higher levels of NHEJ. In contrast, we find that CtIP-K467A does not lead to a concomitant

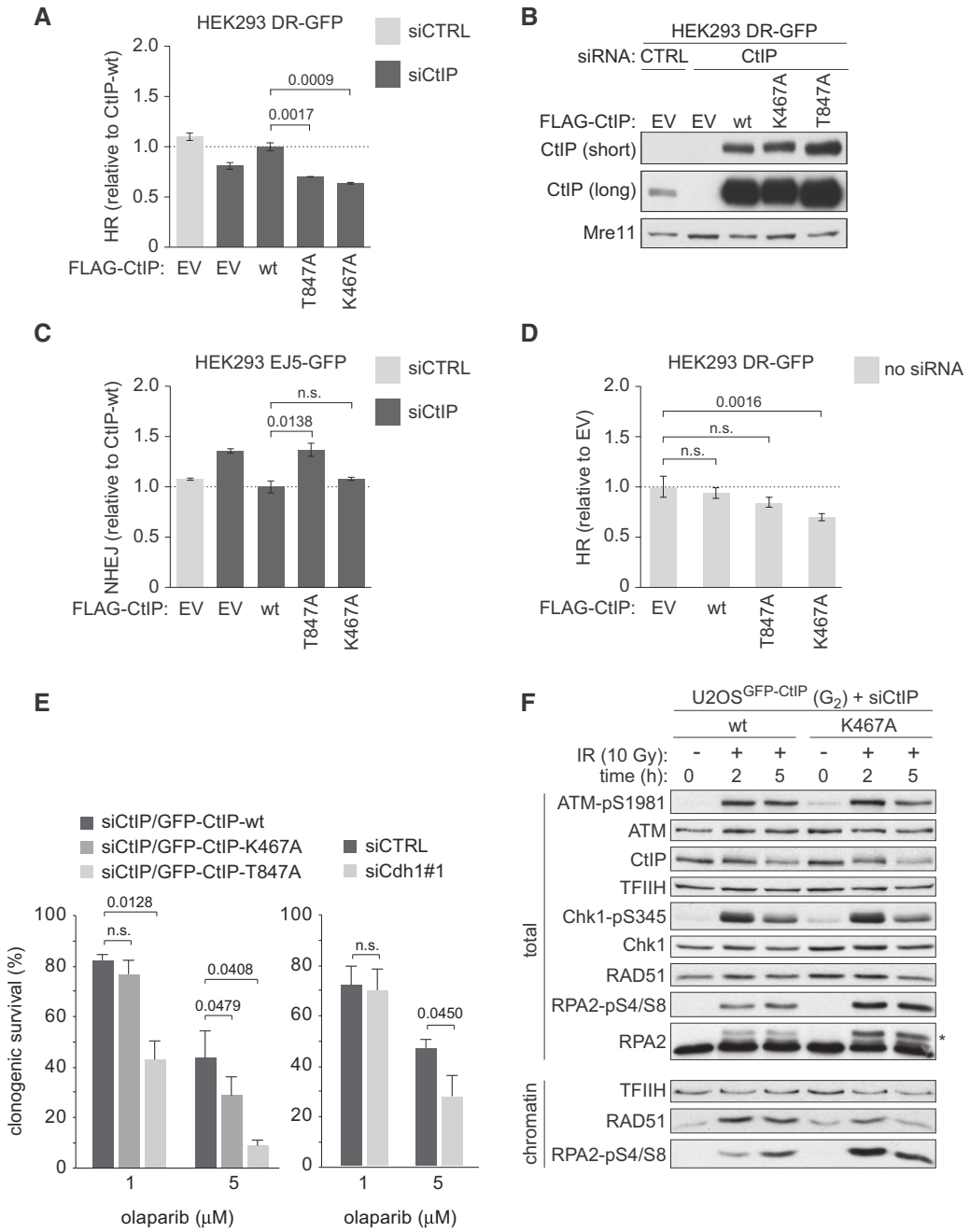


**Figure 8. CtIP–Cdh1 interaction limits DNA-end resection and is required for homologous recombination repair.**

A–D HEK293 cell lines stably harboring DNA repair reporters for HR (DR-GFP; A, B, and D), or NHEJ (EJ5-GFP; C) were transfected with control siRNA, or with CtIP siRNA in combination with the indicated siRNA-resistant FLAG-CtIP plasmids. After 24 h, cells were transfected with the I-*Sce*I-expression plasmid, and 48 h later, GFP positivity was assessed by flow cytometry. Averages and standard deviations of three independent experiments are indicated. In (B), representative Western blots for (A) are shown. Lysates were immunoblotted using anti-CtIP and anti-Mre11 antibodies. HEK293-DR-GFP cells (D) were co-transfected with the indicated siRNA-resistant FLAG-CtIP plasmids together with the I-*Sce*I-expression plasmid. 48 h later, GFP positivity was assessed by flow cytometry.

E U2OS-GFP-CtIP-wt, U2OS-GFP-CtIP-K467A, or U2OS-GFP-CtIP-T847A clones were transfected with siCtIP and were induced to express GFP-CtIP-wt, GFP-CtIP-K467, or GFP-CtIP-T847A at 24 h after transfection. Cells were replated for clonogenic survival 48 h after transfection and treated with the indicated olaparib concentrations. Alternatively, U2OS cells were transfected with siCdh1#1 and replated for clonogenic survival at 48 h after transfection in the presence of the indicated concentrations of olaparib. Standard error of the means of three experiments is shown. Statistical analysis was done using Student's *t*-tests (n.s. indicates not significant).

F U2OS Flp-In T-REx clones stably expressing doxycycline-inducible GFP-CtIP-wt, and GFP-CtIP-K467A were transfected with siCtIP, and protein expression was simultaneously induced by adding doxycycline. After 6 h, cells were synchronized using a single thymidine block for 18 h. Seven hours after release, cells enriched in S/G$_2$ phase (see Supplementary Fig S8D for cell cycle profiles) were mock-treated or harvested at the indicated time points following irradiation. RIPA whole-cell lysates or chromatin-enriched fractions were immunoblotted using the indicated antibodies.

 

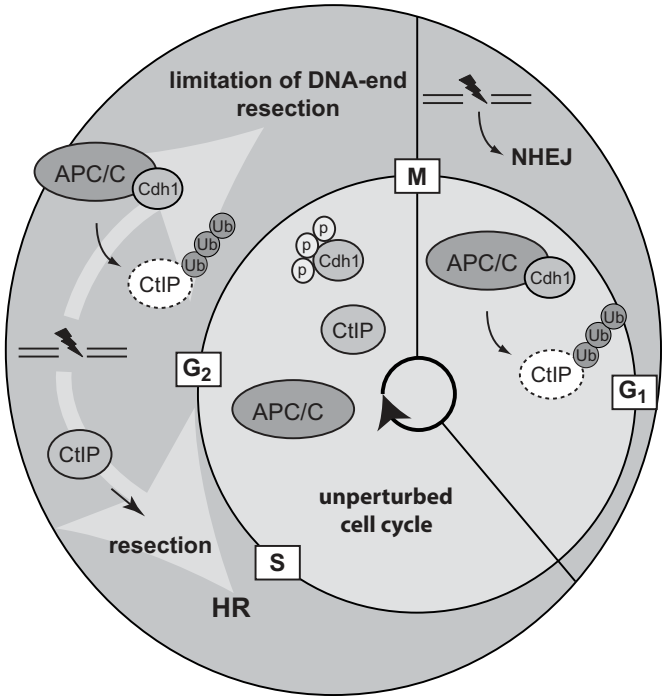


**Figure 9. Model of cell cycle- and DNA damage-dependent regulation of CtIP by the APC/C$^{Cdh1}$.**
The central area represents unperturbed cell cycle, when CtIP is degraded after mitotic exit by the APC/C$^{Cdh1}$. Cells in $G_0/G_1$ lack CDK activity, which precludes phosphorylation and consequent activation of CtIP. Post-mitotic CtIP degradation by the APC/C$^{Cdh1}$ E3 ubiquitin ligase may contribute to prevent unscheduled DNA-end resection in $G_0/G_1$ phase. In response to DSBs in $S/G_2$ phase, CtIP promotes DNA-end resection to facilitate HR repair. In response to high levels of DSBs, CtIP is initially recruited to DSBs to resect DNA ends and promote HR repair. In a late response to high levels of DNA damage, the APC/C$^{Cdh1}$ promotes ubiquitin-dependent proteolysis of CtIP. Downregulation of CtIP by the APC/C$^{Cdh1}$ promotes its clearance from DSBs and prevents excessive DNA-end resection, a prerogative for proper homology-directed repair.

increase in NHEJ, suggesting that resection has occurred in those cells. In fact, CtIP-K467A-expressing cells irradiated in $G_2$ display even heightened levels of DNA-end resection compare to CtIP-wt cells, but are partially impaired in promoting efficient Rad51 recruitment to damaged chromatin, which is similar to what we observed in Cdh1-depleted cells. Moreover, reduced HR efficiency of K467A mutant cells is in line with our data of decreased survival upon PARP inhibition.

Combined, our data support a model in which APC/C$^{Cdh1}$ activity is involved in negatively regulating the stability of CtIP both after mitotic exit in unperturbed cells and after DNA damage in $G_2$ (Fig 9). Moreover, we speculate that the APC/C$^{Cdh1}$ is required at a late stage within the HR process, after initiation of resection has occurred and NHEJ is no longer an option for DSB repair. One possibility is that APC/C$^{Cdh1}$ mediates clearance of CtIP IRIF through ubiquitin-mediated degradation, thereby limiting resection to amounts of ssDNA that can be handled by the downstream recombination machinery. A similar mechanism has been recently reported by Choi *et al* for the regulation of nuclear PTEN, in which Cdh1 promotes the removal of PTEN from chromatin during mitotic exit (Choi *et al*, 2014).

Our observations that Rad51 IRIF are decreased in Cdh1-depleted $G_2$ cells, that CtIP-K467 IRIF persist much longer, and that Rad51 loading onto damaged chromatin is compromised in $G_2$-enriched cells expressing the CtIP KEN box mutant are in line with a role for APC/C$^{Cdh1}$-dependent CtIP degradation in controlling HR. In its role of keeping DNA-end resection in check, the APC/C$^{Cdh1}$ may play a similar function in $G_1$ and $G_2$. In response to DNA breaks in $G_1$ cells, the end resection machinery cannot be activated due to lack of CDK activity. In this context, APC/C$^{Cdh1}$-mediated degradation of CtIP may serve as a backup mechanism to prevent unscheduled end resection. In $G_2$ cells, on the other hand, end resection is required for error-free DSB repair by HR. Here, APC/C$^{Cdh1}$-mediated degradation of CtIP, after initial resection has been performed, may be required to limit end resection to levels that optimally facilitate HR repair.

## Materials and Methods

### Cell culture

hTERT-immortalized retinal pigment epithelium (RPE-1), U2OS, U2OS-FUCCI, and HEK293T cells were grown in DMEM (Gibco, Life Technologies). MCF7 cells were cultured in RPMI (Gibco, Life Technologies). HeLa cells were cultured in DMEM/Ham's F12 (1:1) medium (Gibco, Life Technologies). All culture media were supplemented with 10% fetal calf serum (FCS), 100 units/ml penicillin, and 100 μg/ml streptomycin. U2OS and HEK293 Flp-In T-REx cells were grown in DMEM supplemented with 10% Tet system approved FCS, 100 U/ml penicillin, 100 mg/ml streptomycin, 125 μg/ml hygromycin B, and 12.5 μg/ml blasticidin S.

IR was given using a CIS international/IBL 637 irradiator equipped with a cesium$^{137}$ source (dose rate: 0.01083 Gy/s), or using a Faxitron X-ray device. For serum starvation experiments, RPE-1 cells were initially plated in medium containing 10% FCS and were washed with phosphate-buffered saline (PBS) at 24 h after plating and subsequently cultured without serum for another 24 h. After serum starvation, serum was added to a final concentration of 20%. At the time of serum addition, bromodeoxyuridine (BrdU) was added to a final concentration of 10 μM to measure replication onset. If indicated, cells were treated with 5 μM of the proteasome inhibitor MG-132 (Sigma-Aldrich, St. Louis, MO), 250 nM of the microtubule polymerization inhibitor nocodazole (Sigma-Aldrich), 5 μM of the Eg5 inhibitor *S*-trityl-L-cysteine (STLC, Sigma-Aldrich), 5 μM of the Cdk1 inhibitor RO-3306 (Axon Medchem, Groningen, the Netherlands), or with the APC/C inhibitor proTAME (Zeng *et al*, 2010) at a final concentration of 12 or 20 μM. ProTAME was kindly provided by Randy King, Harvard Medical School, Boston MA, or obtained from Boston Biochem.

### Generation of stable GFP-CtIP cell lines

The Flp-In T-REx system (Invitrogen, Life Technologies) was used to generate cell lines stably expressing different siRNA-resistant GFP-CtIP constructs in an inducible manner. The GFP-CtIP-containing pcDNA5/FRT/TO vector and the Flp recombinase expression plasmid pOG44 were mixed in a 1:9 ratio and transfected into Flp-In T-REx 293 (Invitrogen, Life Technologies) and Flp-In T-REx U2OS (a kind gift of Daniel Durocher, University of Toronto) cells using

FuGENE 6 transfection reagent (Promega) at 60% confluency. After 6 h, medium was exchanged to fresh DMEM and cells were incubated at 30°C (6% $CO_2$). Two days later, cells were replated at different dilutions in 10-cm plates. After 24 h, the medium was supplemented with 250 μg/ml hygromycin B and 12.5 μg/ml blasticidin S. The medium was replaced every 2–3 days, and cells were selected for approximately 2 weeks. Resistant colonies were picked and further characterized as single clones or pooled to generate bulk cultures. All cell lines were screened for inducible GFP-CtIP expression by both immunofluorescence microscopy and immunoblotting. To induce expression of GFP-CtIP, cells were treated with 0.5 or 1 μg/ml doxycycline (Dox) for 24 h as indicated.

#### Immunoprecipitation and GST pull-down

For immunoprecipitation and glutathione S-transferase (GST) pull-down assays, cells were lysed in NP-40 extraction buffer (50 mM Tris–HCl, pH 7.5, 120 mM NaCl, 1 mM EDTA, 6 mM EGTA, 15 mM sodium pyrophosphate, 1% NP-40), supplemented with phosphatase inhibitors (20 mM NaF, 1 mM sodium orthovanadate) and protease inhibitors (1 mM benzamidine and 0.1 mM phenylmethylsulfonyl fluoride (PMSF)), and clarified by centrifugation at 20,000 *g*. HeLa nuclear extracts (HNE) were purchased from Ipracell (Belgium). Generation of the GST–CtIP constructs was described previously (Sartori *et al*, 2007). GST fusion plasmids were grown in BL21 RIL (CodonPlus) *Escherichia coli* (Stratagene), and recombinant proteins were expressed by incubating the bacteria for 24 h at 16°C after the addition of 100 μM IPTG. After centrifugation, the bacterial pellet was resuspended in cold PBS, supplemented with 1% Triton X-100 and protease inhibitors (1 mM PMSF, 1 mM benzamidine, and Roche protease inhibitor cocktail). After sonication and centrifugation, GST-tagged proteins were purified from soluble extracts using Glutathione Sepharose 4 Fast Flow beads (GE Healthcare). GST fusion proteins bound to glutathione beads were mixed with 1 mg of HeLa nuclear extract and incubated for 1 h at 4°C in 1 ml of TEN100 buffer (20 mM Tris–HCl (pH 7.4), 0.1 mM EDTA, and 100 mM NaCl). Beads were then washed three times with NTEN500 buffer (0.5% NP-40, 0.1 mM EDTA, 20 mM Tris–HCl (pH 7.4), and 500 mM NaCl) and once with TEN100 buffer. Recovered complexes were boiled in SDS sample buffer and analyzed by SDS–PAGE followed by immunoblotting.

Immunoprecipitating antibodies were added to the cell lysates and incubated overnight at 4°C. After 2 h incubation with protein A or protein G beads, precipitated immunocomplexes were washed four times with lysis buffer or three times with TNE buffer (50 mM Tris–HCl (pH 7.4), 100 mM NaCl, 0.1 mM EDTA) containing 1% Triton X-100 and once with TNE buffer, boiled in SDS sample buffer, and loaded on an SDS–polyacrylamide gel. Proteins were analyzed by immunoblotting as described below.

#### *In vivo* ubiquitylation assays

HEK293 Flp-In T-REx GFP-CtIP cells were transfected with His-ubiquitin using the FuGENE 6 transfection reagent (Promega), and after 24 h, GFP-CtIP expression was induced with 1 μg/ml Dox. After 24 h, cells were treated for 4 h with 20 μM MG-132 and then washed and scraped in 500 μl of ice-cold PBS. 2% of the cell suspension was used for direct Western blot analysis. The remaining cells were lysed in "buffer A" (6 M guanidine–HCl, 0.1 M $Na_2HPO_4$/$NaH_2PO_4$, pH 8.0, 10 mM imidazole), and lysates were incubated with $Ni^{2+}$-NTA agarose beads for 3 h under rotation at room temperature. The beads were washed two times with buffer A, two times with "buffer A/TI" (1 volume buffer A: 3 volume buffer "TI" (25 mM Tris–HCl, pH 6.8, and 20 mM imidazole)), and two times with buffer TI. Bound proteins were eluted by boiling the beads in 2× SDS sample buffer supplemented with 250 mM imidazole and analyzed by immunoblotting. In case of siRNA treatment, cells were first transfected with the indicated siRNA and after 24 h transfected with His-ubiquitin using the FuGENE6 transfection reagent (Promega). At the same time, GFP-CtIP expression was induced with 1 μg/ml Dox, and after 24 h, samples were processed as described above.

To analyze ubiquitylation of endogenous CtIP, HEK293 cells were transfected with HA-ubiquitin using the FuGENE 6 transfection reagent (Promega) and enriched in $S/G_2$ phase of the cell cycle by releasing them from a single thymidine block. After treatment, cells were lysed in (5 mM Tris–HCl (pH 7.5), 5 mM DTT, 1% SDS) and boiled for 5 min (El-Shemerly *et al*, 2005). After sonication, samples were clarified by centrifugation and diluted 4 times with NP-40 buffer supplemented with phosphatase inhibitors (20 mM NaF, 1 mM sodium orthovanadate), protease inhibitors (1 mM benzamidine and 0.1 mM phenylmethylsulfonyl fluoride (PMSF)), and the deubiquitinases inhibitor N-ethylmaleimide (NEM, 20 mM). Immunoprecipitation was performed overnight at 4°C, using a polyclonal rabbit antibody (612L, raised against CtIP N-terminus, a kind gift of Prof. Richard Baer, Columbia University). After 2 h incubation with protein A beads, precipitated immunocomplexes were washed three times with NTEN500 buffer and once with TEN100 buffer, boiled in SDS sample buffer, and loaded on an SDS–polyacrylamide gel. After transfer, membranes were incubated for 30 min at 4°C in denaturing buffer (6 M guanidine–HCl, 20 mM Tris–HCl (pH 7.5), 1 mM PMSF, and 5 μM β-mercaptoethanol) as described in Penengo *et al* (2006). After extensive washing with TBS-Tween buffer, membranes were incubated with the appropriate antibody and further processed as described below.

#### Immunoblotting

If not specified otherwise, cell extracts were prepared in Laemmli buffer (4% SDS, 20% glycerol, 120 mM Tris–HCl pH 6.8). If indicated, cells were lysed in RIPA buffer (50 mM Tris–HCl, pH 7.5, 1% NP-40, 0.25% sodium deoxycholate, 150 mM NaCl, 1 mM EDTA, and 0.1% SDS) supplemented with phosphatase and protease inhibitors. Proteins were resolved by SDS–PAGE and transferred to nitrocellulose. Immunoblots were performed using the appropriate antibodies, and proteins were visualized using the ECL detection system (Amersham). Primary antibodies used in this study are listed in Supplementary Table S2. The anti-Claspin antibody was a kind gift of Dr. Raimundo Freire, University of Tenerife) and was described previously (Semple *et al*, 2007).

When indicated, a Triton X-100-insoluble (chromatin-enriched) fraction was isolated as described in Peña-Diaz *et al* (2012). Briefly, cells were rinsed twice in cold PBS and incubated for 5 min on ice in pre-extraction buffer (25 mM HEPES (pH 7.9), 50 mM NaCl, 1 mM EDTA, 3 mM $MgCl_2$, 300 mM sucrose, 0.5% Triton X-100, and protease inhibitors). After buffer removal and rinsing in PBS,

 

adherent cellular material was harvested by scraping it into Laemmli buffer. The chromatin-enriched fraction was then heat denatured, sonicated, and analyzed by immunoblotting.

#### HR and NHEJ DNA repair assays

DSB repair efficiency by HR or NHEJ was measured in DR-GFP or EJ5-GFP HEK293 cell lines as described previously (Bennardo *et al*, 2008). Briefly, $0.6 \times 10^6$ cells were plated in 6-well plates (poly-L-lysine coated) and, after 24 h, cells were transfected with siRNA oligos (40 nM). The next day, $0.24 \times 10^6$ cells were reseeded in 12-well plates. At 48 h after siRNA transfection, cells were either mock-transfected or transfected with 0.6 μg I-*Sce*I expression plasmid (pCBASce) in combination with 0.2 μg of the appropriate FLAG-tagged CtIP constructs (pcDNA3) using 1.6 μl of JetPrime (Polyplus). At 4 h after plasmids transfection, media were replaced and a second transfection with siRNA oligos (15 nM) was performed. Alternatively, cells were only transfected with 0.6 μg I-*Sce*I expression plasmid (pCBASce) in combination with 0.2 μg of the appropriate FLAG-tagged CtIP constructs (pcDNA3) using 1.6 μl of JetPrime (Polyplus). At 48 h after I-*Sce*I transfection, cells were analyzed for GFP expression by flow cytometry on a CyAn ADP 9 (Dako).

#### Laser micro-irradiation

Laser micro-irradiation to generate DSBs in a defined nuclear region was performed as described previously (Lukas *et al*, 2003; Bekker-Jensen *et al*, 2006). Briefly, 24 h before irradiation, culture medium was supplemented with 10 μM BrdU. Around 100 cells were micro-irradiated at room temperature (a procedure lasting around 10 min) using the MMI CELLCUT system containing a UVA laser of 355 nm (Molecular Machines and Industries, Zurich, Switzerland). The laser intensity was set to 50% energy output, and each cell was generally exposed to the laser beam for < 300 ms (Meerang *et al*, 2011).

#### DNA plasmids and RNA interference

Plasmids were transfected by using either the standard calcium phosphate method or FuGENE 6 (Promega) according to manufacturer's instructions. The epitope-tagged expression vectors for human CtIP have been described previously (Yu *et al*, 2006; Sartori *et al*, 2007). The HA-tagged expression vector for human Cdh1 was described previously and was purchased from Addgene (plasmid #11596) (Pfleger *et al*, 2001). The pcDNA3.1-6×His-ubiquitin plasmid was a kind gift of Matthias Peter (ETH Zurich, Switzerland), whereas the HA-ubiquitin plasmid was described previously and purchased from Addgene (plasmid #18712) (Kamitani *et al*, 1997). All CtIP point mutants were introduced by site-directed mutagenesis using Expand Long Template PCR System (Roche) and confirmed by sequencing. shRNA interference for Cdh1 in RPE-1, MCF7, or HeLa cells was performed using lentiviral infection with control pLL3.7-GFP (targeting sequence: 5′-GGCATCAAGGTGAACTTCA-3′) or pLL3.7-Cdh1 (targeting sequence: 5′-GGATTAACGAGAATGA GAA-3′; provided by r, University of Freiburg, Germany) (Engelbert *et al*, 2008). To this end, HEK293T cells were transfected with the pLL3.7 plasmids along with the packaging plasmids pCMV-VSVG, pCMV-dR8.2 (provided by Robert Weinberg, MIT, Cambridge, MA), and pAdVAntage (Promega) in a 4:3:1:0.5 ratio. Virus-containing supernatant was harvested at 24 and 48 h after transfection, filtered through a 0.45-μM syringe filter, and used to infect target cells, which were subsequently selected with 1 μg/ml puromycin. Analysis of stable Cdh1-depleted cells was done at 5 days post-infection.

For transient siRNA experiments, RPE-1, MCF7, HeLa, or U2OS cells were plated in 6-well plates and transfected with the indicated amounts of siRNA oligos (40 nM final concentration of oligos) using Oligofectamine or Lipofectamine RNAiMAX using manufacturer's guidelines (Invitrogen, Life Technologies). In brief, medium was replaced with Opti-MEM (Gibco, Life Technologies) prior to incubation with siRNAs and Oligofectamine for 4 h. Thereafter, medium containing FCS (10% final concentration) was added and cells were analyzed at 48 or 72 h after transfection. siRNA oligos targeting Cdh1 #1 (5′-GGATTAACGAGAATGAGAAdTdT-3′), Cdh1 #2 (5′-AA TGAGAAGTCTCCCAGTCAGdTdT-3′), CtIP (5′-GCUAAACAGGAACG AAUCTTdTdT-3′) (Sartori *et al*, 2007), or luciferase (5′-CGUACGCG GAAUACUUCGAdTdT-3′) were purchased from Ambion (Life Technologies) or Microsynth (Balgach, Switzerland). In addition, "medium GC duplex" control siRNA (Cat. No: 12935-300) was purchased from Ambion (Life Technologies).

#### SILAC and mass spectrometry

For SILAC experiments, RPE-1 cells were cultured in ready-to-use light and heavy DMEM media, containing light or heavy arginine and lysine ("R0K0 DMEM" with $^{12}C_6$-L-arginine and $^{12}C_6$-L-lysine or "R10K8 DMEM" with $^{13}C_6$-L-arginine and $^{13}C_6$-L-lysine, respectively) and supplemented with dialyzed FBS. Media were obtained from Silantes (Munich, Germany). SILAC labeling was performed as previously described by Ong and Mann (Ong *et al*, 2002). Briefly, RPE-1 cells were cultured in normal media or complete heavy DMEM medium containing 10% dialyzed FBS for at least 10 cell doublings (5 passages) to allow full incorporation of both labeled amino acids within the proteome. Cells were subsequently treated with nocodazole for 16 h (250 ng/ml) and collected by mitotic shake-off. Cells were washed three times in pre-warmed PBS and replated in the absence of nocodazole. Immediately after replating or 2.5 h after replating, cells were harvested by trypsinization, snap-frozen in liquid nitrogen, and resuspended in lysis buffer (6 M urea and 2 M thio-urea). A label-swap replicate was also performed where SILAC states and harvesting conditions were reversed (Fig 3A). To determine protein concentration in lysates, 10 μl lysate was added to 150 μl of 660 nM protein assay reagent (Pierce). Equal amounts of protein from R0K0 and R10K8 were mixed, reduced with 1 mM DTT, and alkylated with 8 mM iodoacetamide. Proteins were separated on SDS–PAGE 4–12% gradient gels and visualized by staining by Coomassie staining. Gel lanes were divided into eight slices and proteins digested with an in-gel digestion protocol with trypsin. Peptides were desalted on C18 StageTips and loaded on a 10-cm-long 360 μm O.D. by 75 μm I.D. column packed with 3 μm ReproSil-Pur C18 AQ 3beads (Dr. Maisch, Germany) with an Agilent 1100 nano-flow pump and autosampler. A 60 min gradient from 3 to 35% acetonitrile containing 1% formic acid at 200 nl/min was applied to elute peptides for analysis in the LTQ-Orbitrap-Velos (Thermo, Bremen) in a Top5 CID data-dependent acquisition mode. Peptide identification and quantification was performed using MaxQuant v.1.1.1.14 with the IPI human database ver. 3.70 with

variable modifications of oxidized methionine and acetylated protein N-termini. Cysteines were carbamidomethylated. Peptide and protein FDR was set at 1%.

#### Flow cytometry

Cells were harvested at the indicated time points after treatment and fixed in ice-cold 70% ethanol. Cells were stained with rabbit anti-phospho-histone H3 antibody, mouse anti-MPM-2, and/or mouse anti-γ-H2AX (details of used antibodies are in Supplementary Table S2), subsequently stained with Alexa488-conjugated and Alexa647-conjugated secondary antibodies (Molecular Probes, 1:300), and counterstained with propidium iodide/RNase (Sigma). Samples were analyzed on a FACS-Calibur (Becton Dickinson) equipped with Cell Quest software. Per sample, a minimum of $10^4$ events was analyzed and indicated results show averages and standard deviations of three independent experiments.

#### Immunofluorescence microscopy

MCF7, MEFs, or HeLa cells were cultured on glass coverslips and, if indicated, were irradiated at 24 h after plating. After treatment, cells were fixed in formaldehyde (3.7% in PBS) for 15 min at room temperature. After washing with PBS, cells were permeabilized with Triton X-100 (0.1% in PBS) for 5 min at room temperature. After extensive washing, cells were stained with mouse anti-Cdh1, mouse anti-p53 diluted in PBS, 0.05%Tween-20, 2.5%BSA for 16 h at 4°C. After extensive washing, cells were stained with Alexa488-, Alexa568-, or Alexa647-conjugated secondary antibodies for 30 min at room temperature and counterstained with DAPI. Images were obtained using a Leica DM6000B microscope, equipped with 63× immersion lens (PL-S-APO, numerical aperture: 1.30) and Xenon light source using LAS-AF software (Leica).

Alternatively, U2OS-FUCCI cells were grown on glass coverslips and, at different time points after treatment, fixed directly in 4% formaldehyde (w/v) in PBS for 15 min as described previously (Eid *et al*, 2010). After incubation with rabbit anti-Rad51 or rabbit anti-53BP1 and appropriate secondary antibodies the coverslips were mounted and sealed with Vectashield (Vector Laboratories) containing DAPI. Images were acquired on a Leica DMRB fluorescence microscope.

For live-cell microscopy, stable U2OS cells were plated in chambered coverglass 8-well plates (LabTek-II, Nunc). At 24 h before imaging, GFP-CtIP expression was induced by adding doxycycline to a final concentration of 1 μg/ml. GFP and DIC images were obtained every 5 min on a DeltaVision Elite microscope, equipped with a CoolSNAP HQ2 camera, 40× immersion objective (U-APO 340, numerical aperture: 1.35). In the Z-plane, 12 images were acquired at 0.5-μm interval, which were subsequently deconvolved using SoftWorx 5.5 software (Applied Precision). Nuclear fluorescence intensity was quantified using ImageJ software.

#### Clonogenic and short-term survival assays

HeLa or MCF7 cells were cultured in 6-well plates. One day after plating, cells were irradiated with 1, 2, or 4 Gy. When surviving colonies were approximately 50 cells in size, cells were fixed and stained using methanol/acidic acid/water in a 5:2:3 ratio, supplemented with 0.01% Coomassie brilliant blue. Surviving fractions were calculated using the plating efficiencies with non-irradiated conditions as a reference. Shown averages are from three experiments, with three replicates each. Alternatively, clonal U2OS cells expressing GFP-CtIP variants were transfected with siRNAs and, if indicated, were treated with doxycycline 24 h later to induce expression of GFP-CtIP. At 48 h after transfection, cells were trypsinized and replated in 6-well plates. During replating, indicated doses of doxorubicin or the PARP inhibitor olaparib (Axon Medchem, Groningen, the Netherlands) were added. To test whether Cdh1-depleted cells also are more sensitive to PARP inhibition, U2OS cells were transfected with siCdh1#1, and after 48 h, cells were replated in the presence of olaparib. Statistical testing was done using the Student's *t*-test.

For short-term survival assays, 2,000 cells were plated in 96-wells plates and treated at 24 h after plating. At 4 days after treatment initiation, 20 μl of 3-(4,5-dimethylthiazol-2-yl)-2,5-diphenyltetrazolium bromide (MTT) was added to the culture medium to a final concentration of 5 mg/ml for 3 h. Formazan crystals were dissolved in DMSO, and absorbance was analyzed at 520 nM using a Bio-Rad benchmark III microtiter spectrophotometer. Survival was calculated as a percentage of untreated cells.

#### Gene set enrichment analysis (GSEA) and destruction motif analysis

GSEA was performed with GSEA 2.0 (Broad Institute, Cambridge, MA) (Mootha *et al*, 2003; Subramanian *et al*, 2005). A significance threshold was set at a nominal *P*-value of 0.05 and a false discovery rate (FDR) of 0.30. In our analysis, we transformed protein names from SILAC MS analysis to HUGO gene symbols and tested enrichment in Kyoto Encyclopedia of Genes and Genomes (KEGG), Gene Map Annotator and Pathway Profiler (GenMAPP) (Dahlquist *et al*, 2002; Kanehisa *et al*, 2012), and the BioCarta database (http://www.biocarta.com). Within the set of identified proteins from the SILAC MS analysis, we used GPS-ARM (Liu *et al*, 2012) to identify proteins with a D-box or a KEN box using a threshold setting of "high" for D-boxes and "medium" for KEN boxes. Subsequently, GSEA was used to test for enrichment of KEN box or D-box containing proteins in the downregulated fraction. FDR rates of 0.25 were used in combination with 10,000 permutations. Conservation of KEN or D-boxes was done using Clustal Omega. In order to identify proteins related to the DNA damage response and DNA damage repair, a combined list of genes was compiled by merging the following Gene Ontology gene sets (see also Supplementary Table S1): GO:0006302 ("double-strand break repair); GO:0006974 ("cellular response to DNA damage stimulus"); GO:0000077 ("DNA damage checkpoint"); and GO:0000724 ("double-strand repair via homologous recombination"). In total, 255 genes were included in this combined gene set (Supplementary Table S1), which in Fig 3 is referred to as "DNA damage response".

**Supplementary information** for this article is available online: http://emboj.embopress.org

## Acknowledgements

We thank Dr. Rudolf Fehrmann, Dr. Małgorzata Krajewska, and Anne Margriet Heijink for technical help and Dr. Floris Foijer for help with

 

live-cell microscopy. We are grateful to Dr. Jeremy Stark, Dr. Robert Weinberg, Dr. Ralph Waesch, Dr. Stefano Ferrari, Dr. Randy King, Dr. Richard Baer, Dr. Raimundo Freire, and Dr. Matthias Peter for providing reagents. We thank Chris Soon Heng Tan and Rob Wolthuis for helpful discussions. This research was supported by an NWO-VIDI grant (016.136.334) and Dutch Cancer Society grant (RUG-2011-5093) to M.A.T.M.v.V, an ERC Advanced Grant to E.G.E.d.V (ERC-2011-293445). Alessandro A. Sartori is supported by the Vontobel-Stiftung. Lorenzo Lafranchi is supported by grants of the Swiss National Science Foundation (31003A_135507 to A.A.S) and the Promedica Stiftung (to A.A.S).

### Author contributions

LL and HRdB performed experiments, analyzed the data, and edited the manuscript. SEO performed mass spectrometry analyses. EGEdV edited the manuscript. AAS and MATMvV directed and supervised the studies, analyzed the data, and wrote the manuscript.

### Conflict of interest

The authors declare that they have no conflict of interest.

## References

Acilan C, Potter DM, Saunders WS (2007) DNA repair pathways involved in anaphase bridge formation. *Genes Chromosom Cancer* 46: 522 – 531

Aylon Y, Liefshitz B, Kupiec M (2004) The CDK regulates repair of double-strand breaks by homologous recombination during the cell cycle. *EMBO J* 23: 4868 – 4875

Ayoub N, Rajendra E, Su X, Jeyasekharan AD, Mahen R, Venkitaraman AR (2009) The carboxyl terminus of Brca2 links the disassembly of Rad51 complexes to mitotic entry. *Curr Biol* 19: 1075 – 1085

Bassermann F, Frescas D, Guardavaccaro D, Busino L, Peschiaroli A, Pagano M (2008) The Cdc14B-Cdh1-Plk1 axis controls the G2 DNA-damage-response checkpoint. *Cell* 134: 256 – 267

Bekker-Jensen S, Lukas C, Kitagawa R, Melander F, Kastan MB, Bartek J, Lukas J (2006) Spatial organization of the mammalian genome surveillance machinery in response to DNA strand breaks. *J Cell Biol* 173: 195 – 206

Bennardo N, Cheng A, Huang N, Stark JM (2008) Alternative-NHEJ is a mechanistically distinct pathway of mammalian chromosome break repair. *PLoS Genet* 4: e1000110

Bonneau AM, Sonenberg N (1987) Involvement of the 24-kDa cap-binding protein in regulation of protein synthesis in mitosis. *J Biol Chem* 262: 11134 – 11139

Bryant HE, Schultz N, Thomas HD, Parker KM, Flower D, Lopez E, Kyle S, Meuth M, Curtin NJ, Helleday T (2005) Specific killing of BRCA2-deficient tumours with inhibitors of poly(ADP-ribose) polymerase. *Nature* 434: 913 – 917

Chan K-L, North PS, Hickson ID (2007) BLM is required for faithful chromosome segregation and its localization defines a class of ultrafine anaphase bridges. *EMBO J* 26: 3397 – 3409

Chapman JR, Taylor MRG, Boulton SJ (2012) Playing the end game: DNA double-strand break repair pathway choice. *Mol Cell* 47: 497 – 510

Choi BH, Pagano M, Huang C, Dai W (2014) Cdh1, a substrate-recruiting component of anaphase-promoting complex/cyclosome (APC/C) ubiquitin E3 ligase, specifically interacts with phosphatase and tensin homolog (PTEN) and promotes its removal from chromatin. *J Biol Chem* 289: 17951 – 17959

Dahlquist KD, Salomonis N, Vranizan K, Lawlor SC, Conklin BR (2002) GenMAPP, a new tool for viewing and analyzing microarray data on biological pathways. *Nat Genet* 31: 19 – 20

Delgado-Esteban M, García-Higuera I, Maestre C, Moreno S, Almeida A (2013) APC/C-Cdh1 coordinates neurogenesis and cortical size during development. *Nat Commun* 4: 2879

Eguren M, Porlan E, Manchado E, García-Higuera I, Cañamero M, Fariñas I, Malumbres M (2013) The APC/C cofactor Cdh1 prevents replicative stress and p53-dependent cell death in neural progenitors. *Nat Commun* 4: 2880

Eguren M, Álvarez-Fernández M, García F, López-Contreras AJ, Fujimitsu K, Yaguchi H, Luque-García JL, Fernandez-Capetillo O, Muñoz J, Yamano H, Malumbres M (2014) A synthetic lethal interaction between APC/C and topoisomerase poisons uncovered by proteomic screens. *Cell Rep* 6: 670 – 683

Eid W, Steger M, El-Shemerly M, Ferretti LP, Peña-Diaz J, König C, Valtorta E, Sartori AA, Ferrari S (2010) DNA end resection by CtIP and exonuclease 1 prevents genomic instability. *EMBO Rep* 11: 962 – 968

El-Shemerly M, Janscak P, Hess D, Jiricny J, Ferrari S (2005) Degradation of human exonuclease 1b upon DNA synthesis inhibition. *Cancer Res* 65: 3604 – 3609

Emanuele MJ, Ciccia A, Elia AEH, Elledge SJ (2011) Proliferating cell nuclear antigen (PCNA)-associated KIAA0101/PAF15 protein is a cell cycle-regulated anaphase-promoting complex/cyclosome substrate. *Proc Natl Acad Sci USA* 108: 9845 – 9850

Engelbert D, Schnerch D, Baumgarten A, Wäsch R (2008) The ubiquitin ligase APC(Cdh1) is required to maintain genome integrity in primary human cells. *Oncogene* 27: 907 – 917

Esashi F, Christ N, Gannon J, Liu Y, Hunt T, Jasin M, West SC (2005) CDK-dependent phosphorylation of BRCA2 as a regulatory mechanism for recombinational repair. *Nature* 434: 598 – 604

Falck J, Forment JV, Coates J, Mistrik M, Lukas J, Bartek J, Jackson SP (2012) CDK targeting of NBS1 promotes DNA-end resection, replication restart and homologous recombination. *EMBO Rep* 13: 561 – 568

Farmer H, McCabe N, Lord CJ, Tutt ANJ, Johnson DA, Richardson TB, Santarosa M, Dillon KJ, Hickson I, Knights C, Martin NMB, Jackson SP, Smith GCM, Ashworth A (2005) Targeting the DNA repair defect in BRCA mutant cells as a therapeutic strategy. *Nature* 434: 917 – 921

Ferreira MG, Cooper JP (2004) Two modes of DNA double-strand break repair are reciprocally regulated through the fission yeast cell cycle. *Genes Dev* 18: 2249 – 2254

Ferretti LP, Lafranchi L, Sartori AA (2013) Controlling DNA-end resection: a new task for CDKs. *Front Genet* 4: 99

French JD, Dunn J, Smart CE, Manning N, Brown MA (2006) Disruption of BRCA1 function results in telomere lengthening and increased anaphase bridge formation in immortalized cell lines. *Genes Chromosom Cancer* 45: 277 – 289

García-Higuera I, Manchado E, Dubus P, Cañamero M, Méndez J, Moreno S, Malumbres M (2008) Genomic stability and tumour suppression by the APC/C cofactor Cdh1. *Nat Cell Biol* 10: 802 – 811

Gudas JM, Li T, Nguyen H, Jensen D, Rauscher FJ, Cowan KH (1996) Cell cycle regulation of BRCA1 messenger RNA in human breast epithelial cells. *Cell Growth Differ* 7: 717 – 723

He J, Chao WCH, Zhang Z, Yang J, Cronin N, Barford D (2013) Insights into degron recognition by APC/C coactivators from the structure of an Acm1-Cdh1 complex. *Mol Cell* 50: 649 – 660

Henderson KA, Kee K, Maleki S, Santini PA, Keeney S (2006) Cyclin-dependent kinase directly regulates initiation of meiotic recombination. *Cell* 125: 1321 – 1332

Huertas P, Jackson SP (2009) Human CtIP mediates cell cycle control of DNA end resection and double strand break repair. *J Biol Chem* 284: 9558 – 9565

Ira G, Pellicioli A, Balijja A, Wang X, Fiorani S, Carotenuto W, Liberi G, Bressan D, Wan L, Hollingsworth NM, Haber JE, Foiani M (2004) DNA end resection, homologous recombination and DNA damage checkpoint activation require CDK1. *Nature* 431: 1011 – 1017

Jackson SP, Bartek J (2009) The DNA-damage response in human biology and disease. *Nature* 461: 1071 – 1078

Jazayeri A, Falck J, Lukas C, Bartek J, Smith GCM, Lukas J, Jackson SP (2006) ATM- and cell cycle-dependent regulation of ATR in response to DNA double-strand breaks. *Nat Cell Biol* 8: 37 – 45

Johnson N, Li Y-C, Walton ZE, Cheng KA, Li D, Rodig SJ, Moreau LA, Unitt C, Bronson RT, Thomas HD, Newell DR, D'Andrea AD, Curtin NJ, Wong K-K, Shapiro GI (2011) Compromised CDK1 activity sensitizes BRCA-proficient cancers to PARP inhibition. *Nat Med* 17: 875 – 882

Kaidi A, Weinert BT, Choudhary C, Jackson SP (2010) Human SIRT6 promotes DNA end resection through CtIP deacetylation. *Science* 329: 1348 – 1353

Kamitani T, Kito K, Nguyen HP, Yeh ET (1997) Characterization of NEDD8, a developmentally down-regulated ubiquitin-like protein. *J Biol Chem* 272: 28557 – 28562

Kanehisa M, Goto S, Sato Y, Furumichi M, Tanabe M (2012) KEGG for integration and interpretation of large-scale molecular data sets. *Nucleic Acids Res* 40: D109 – D114

Kousholt AN, Fugger K, Hoffmann S, Larsen BD, Menzel T, Sartori AA, Sørensen CS (2012) CtIP-dependent DNA resection is required for DNA damage checkpoint maintenance but not initiation. *J Cell Biol* 197: 869 – 876

Kramer ER, Scheuringer N, Podtelejnikov AV, Mann M, Peters JM (2000) Mitotic regulation of the APC activator proteins CDC20 and CDH1. *Mol Biol Cell* 11: 1555 – 1569

Kumar R, Cheok CF (2014) RIF1: a novel regulatory factor for DNA replication and DNA damage response signaling. *DNA Repair* 15: 54 – 59

Laulier C, Cheng A, Stark JM (2011) The relative efficiency of homology-directed repair has distinct effects on proper anaphase chromosome separation. *Nucleic Acids Res* 39: 5935 – 5944

Lieber MR (2010) The mechanism of double-strand DNA break repair by the nonhomologous DNA end-joining pathway. *Annu Rev Biochem* 79: 181 – 211

Lindon C, Pines J (2004) Ordered proteolysis in anaphase inactivates Plk1 to contribute to proper mitotic exit in human cells. *J Cell Biol* 164: 233 – 241

Littlepage LE, Ruderman JV (2002) Identification of a new APC/C recognition domain, the A box, which is required for the Cdh1-dependent destruction of the kinase Aurora-A during mitotic exit. *Genes Dev* 16: 2274 – 2285

Liu Z, Yuan F, Ren J, Cao J, Zhou Y, Yang Q, Xue Y (2012) GPS-ARM: computational analysis of the APC/C recognition motif by predicting D-boxes and KEN-boxes. *PLoS ONE* 7: e34370

Lukas C, Sørensen CS, Kramer E, Santoni-Rugiu E, Lindeneg C, Peters JM, Bartek J, Lukas J (1999) Accumulation of cyclin B1 requires E2F and cyclin-A-dependent rearrangement of the anaphase-promoting complex. *Nature* 401: 815 – 818

Lukas C, Falck J, Bartkova J, Bartek J, Lukas J (2003) Distinct spatiotemporal dynamics of mammalian checkpoint regulators induced by DNA damage. *Nat Cell Biol* 5: 255 – 260

Meerang M, Ritz D, Paliwal S, Garajova Z, Bosshard M, Mailand N, Janscak P, Hübscher U, Meyer H, Ramadan K (2011) The ubiquitin-selective segregase VCP/p97 orchestrates the response to DNA double-strand breaks. *Nat Cell Biol* 13: 1376 – 1382

Miller JJ, Summers MK, Hansen DV, Nachury MV, Lehman NL, Loktev A, Jackson PK (2006) Emi1 stably binds and inhibits the anaphase-promoting complex/cyclosome as a pseudosubstrate inhibitor. *Genes Dev* 20: 2410 – 2420

Mocciaro A, Berdougo E, Zeng K, Black E, Vagnarelli P, Earnshaw W, Gillespie D, Jallepalli P, Schiebel E (2010) Vertebrate cells genetically deficient for Cdc14A or Cdc14B retain DNA damage checkpoint proficiency but are impaired in DNA repair. *J Cell Biol* 189: 631 – 639

Mootha VK, Lepage P, Miller K, Bunkenborg J, Reich M, Hjerrild M, Delmonte T, Villeneuve A, Sladek R, Xu F, Mitchell GA, Morin C, Mann M, Hudson TJ, Robinson B, Rioux JD, Lander ES (2003) Identification of a gene causing human cytochrome c oxidase deficiency by integrative genomics. *Proc Natl Acad Sci USA* 100: 605 – 610

Nguyen HG, Chinnappan D, Urano T, Ravid K (2005) Mechanism of Aurora-B degradation and its dependency on intact KEN and A-boxes: identification of an aneuploidy-promoting property. *Mol Cell Biol* 25: 4977 – 4992

Ong S-E, Blagoev B, Kratchmarova I, Kristensen DB, Steen H, Pandey A, Mann M (2002) Stable isotope labeling by amino acids in cell culture, SILAC, as a simple and accurate approach to expression proteomics. *Mol Cell Proteomics* 1: 376 – 386

Peña-Diaz J, Bregenhorn S, Ghodgaonkar M, Follonier C, Artola-Borán M, Castor D, Lopes M, Sartori AA, Jiricny J (2012) Noncanonical mismatch repair as a source of genomic instability in human cells. *Mol Cell* 47: 669 – 680

Penengo L, Mapelli M, Murachelli AG, Confalonieri S, Magri L, Musacchio A, Di Fiore PP, Polo S, Schneider TR (2006) Crystal structure of the ubiquitin binding domains of rabex-5 reveals two modes of interaction with ubiquitin. *Cell* 124: 1183 – 1195

Pesin JA, Orr-Weaver TL (2008) Regulation of APC/C activators in mitosis and meiosis. *Annu Rev Cell Dev Biol* 24: 475 – 499

Peters J-M (2006) The anaphase promoting complex/cyclosome: a machine designed to destroy. *Nat Rev Mol Cell Biol* 7: 644 – 656

Pfleger CM, Kirschner MW (2000) The KEN box: an APC recognition signal distinct from the D box targeted by Cdh1. *Genes Dev* 14: 655 – 665

Pfleger CM, Lee E, Kirschner MW (2001) Substrate recognition by the Cdc20 and Cdh1 components of the anaphase-promoting complex. *Genes Dev* 15: 2396 – 2407

Pines J (2011) Cubism and the cell cycle: the many faces of the APC/C. *Nat Rev Mol Cell Biol* 12: 427 – 438

Prescott DM, Bender MA (1963) Autoradiographic study of chromatid distribution of labeled DNA in two types of mammalian cells *in vitro*. *Exp Cell Res* 29: 430 – 442

Rape M, Kirschner MW (2004) Autonomous regulation of the anaphase-promoting complex couples mitosis to S-phase entry. *Nature* 432: 588 – 595

Sakaue-Sawano A, Kurokawa H, Morimura T, Hanyu A, Hama H, Osawa H, Kashiwagi S, Fukami K, Miyata T, Miyoshi H, Imamura T, Ogawa M, Masai H, Miyawaki A (2008) Visualizing spatiotemporal dynamics of multicellular cell-cycle progression. *Cell* 132: 487 – 498

Sartori AA, Lukas C, Coates J, Mistrik M, Fu S, Bartek J, Baer R, Lukas J, Jackson SP (2007) Human CtIP promotes DNA end resection. *Nature* 450: 509 – 514

Semple JI, Smits VAJ, Fernaud J-R, Mamely I, Freire R (2007) Cleavage and degradation of Claspin during apoptosis by caspases and the proteasome. *Cell Death Differ* 14: 1433 – 1442

Shibata A, Conrad S, Birraux J, Geuting V, Barton O, Ismail A, Kakarougkas A, Meek K, Taucher-Scholz G, Löbrich M, Jeggo PA (2011) Factors determining DNA double-strand break repair pathway choice in G2 phase. *EMBO J* 30: 1079 – 1092

 

Sigl R, Wandke C, Rauch V, Kirk J, Hunt T, Geley S (2009) Loss of the mammalian APC/C activator FZR1 shortens G1 and lengthens S phase but has little effect on exit from mitosis. *J Cell Sci* 122: 4208 – 4217

Sonoda E, Hochegger H, Saberi A, Taniguchi Y, Takeda S (2006) Differential usage of non-homologous end-joining and homologous recombination in double strand break repair. *DNA Repair* 5: 1021 – 1029

Steger M, Murina O, Hühn D, Ferretti LP, Walser R, Hänggi K, Lafranchi L, Neugebauer C, Paliwal S, Janscak P, Gerrits B, Del Sal G, Zerbe O, Sartori AA (2013) Prolyl isomerase PIN1 regulates DNA double-strand break repair by counteracting DNA end resection. *Mol Cell* 50: 333 – 343

Stewart S, Fang G (2005) Destruction box-dependent degradation of aurora B is mediated by the anaphase-promoting complex/cyclosome and Cdh1. *Cancer Res* 65: 8730 – 8735

Subramanian A, Tamayo P, Mootha VK, Mukherjee S, Ebert BL, Gillette MA, Paulovich A, Pomeroy SL, Golub TR, Lander ES, Mesirov JP (2005) Gene set enrichment analysis: a knowledge-based approach for interpreting genome-wide expression profiles. *Proc Natl Acad Sci USA* 102: 15545 – 15550

Sudo T, Ota Y, Kotani S, Nakao M, Takami Y, Takeda S, Saya H (2001) Activation of Cdh1-dependent APC is required for G1 cell cycle arrest and DNA damage-induced G2 checkpoint in vertebrate cells. *EMBO J* 20: 6499 – 6508

Taguchi SI, Honda K, Sugiura K, Yamaguchi A, Furukawa K, Urano T (2002) Degradation of human Aurora-A protein kinase is mediated by hCdh1. *FEBS Lett* 519: 59 – 65

Trickey M, Grimaldi M, Yamano H (2008) The anaphase-promoting complex/cyclosome controls repair and recombination by ubiquitylating Rhp54 in fission yeast. *Mol Cell Biol* 28: 3905 – 3916

van Vugt MATM, Bràs A, Medema RH (2004) Polo-like kinase-1 controls recovery from a G2 DNA damage-induced arrest in mammalian cells. *Mol Cell* 15: 799 – 811

Wäsch R, Engelbert D (2005) Anaphase-promoting complex-dependent proteolysis of cell cycle regulators and genomic instability of cancer cells. *Oncogene* 24: 1 – 10

White DE, Negorev D, Peng H, Ivanov AV, Maul GG, Rauscher FJ (2006) KAP1, a novel substrate for PIKK family members, colocalizes with numerous damage response factors at DNA lesions. *Cancer Res* 66: 11594 – 11599

Wiebusch L, Hagemeier C (2010) p53- and p21-dependent premature APC/C-Cdh1 activation in G2 is part of the long-term response to genotoxic stress. *Oncogene* 29: 3477 – 3489

Yamamoto A, Taki T, Yagi H, Habu T, Yoshida K, Yoshimura Y, Yamamoto K, Matsushiro A, Nishimune Y, Morita T (1996) Cell cycle-dependent expression of the mouse Rad51 gene in proliferating cells. *Mol Gen Genet* 251: 1 – 12

Yu X, Fu S, Lai M, Baer R, Chen J (2006) BRCA1 ubiquitinates its phosphorylation-dependent binding partner CtIP. *Genes Dev* 20: 1721 – 1726

Zeng X, Sigoillot F, Gaur S, Choi S, Pfaff KL, Oh D-C, Hathaway N, Dimova N, Cuny GD, King RW (2010) Pharmacologic inhibition of the anaphase-promoting complex induces a spindle checkpoint-dependent mitotic arrest in the absence of spindle damage. *Cancer Cell* 18: 382 – 395

Zhang L, Park C-H, Wu J, Kim H, Liu W, Fujita T, Balasubramani M, Schreiber EM, Wang X-F, Wan Y (2010) Proteolysis of Rad17 by Cdh1/APC regulates checkpoint termination and recovery from genotoxic stress. *EMBO J* 29: 1726 – 1737

Ziv Y, Bielopolski D, Galanty Y, Lukas C, Taya Y, Schultz DC, Lukas J, Bekker-Jensen S, Bartek J, Shiloh Y (2006) Chromatin relaxation in response to DNA double-strand breaks is modulated by a novel ATM- and KAP-1 dependent pathway. *Nat Cell Biol* 8: 870 – 876